Title

ωB97X-V: A 10-parameter, range-separated hybrid, generalized gradient approximation density functional with nonlocal correlation, designed by a survival-of-the-fittest strategy

Journal

Physical Chemistry Chemical Physics, 16(21)

ISSN

1463-9076

Authors

Mardirossian, Narbe

Head-Gordon, Martin

Publication Date

2014

DOI

10.1039/c3cp54374a

Peer reviewed

ωB97X-V: A 10-parameter, range-separated hybrid, generalized gradient approximation density functional with nonlocal correlation, designed by a survival-of-the-fittest strategy

Narbe Mardirossian[†] and Martin Head-Gordon[*,†]

†*Department of Chemistry, University of California, Berkeley*
‡*Chemical Sciences Division, Lawrence Berkeley National Laboratory, Berkeley, CA 94720 USA*

E-mail: mhg@cchem.berkeley.edu

Abstract

A 10-parameter, range-separated hybrid (RSH), generalized gradient approximation (GGA) density functional with nonlocal correlation (VV10) is presented. Instead of truncating the B97-type power series inhomogeneity correction factors (ICF) for the exchange, same-spin correlation, and opposite-spin correlation functionals uniformly, all 16383 combinations of the linear parameters up to fourth order ($m = 4$) are considered. These functionals are individually fit to a training set and the resulting parameters are validated on a primary test set in order to identify the 3 optimal ICF expansions. Through this procedure, it is discovered that the functional that performs best on the training *and* primary test sets has 7 linear parameters, with 3 additional nonlinear parameters from range-separation and nonlocal correlation. The resulting density functional, ωB97X-V, is further assessed on a secondary test set, the parallel-displaced coronene dimer, as well as several geometry datasets. Furthermore, the basis set dependence and integration grid sensitivity of ωB97X-V are analyzed and documented in order to facilitate the use of the functional.

1 Introduction

1.1 Background

In the early 1950s, John Slater introduced the first semi-empirical exchange-only density functional: the X-α method.[1] Since then, hundreds of parameterized density functionals have been developed, expanding upon the simplicity of Slater's functional. While the X-α method depended solely on the electron density, its successors have taken into account both the gradient and Laplacian of the electron density, the kinetic energy density, occupied orbitals through exact exchange, and even virtual orbitals through post-Hartree–Fock methods such as MP2. However, almost 50 years after the advent of Kohn–Sham DFT,[2,3] the exact exchange-correlation functional remains elusive. Whereas Slater's functional only had 1 optimizable parameter, today's density functionals can have more than 40 parameters.

While including more parameters in the functional optimization guarantees better performance on the training set, the most desirable attribute of a parameterized density functional is the promise of transferability, and a functional with *less* parameters is more likely to be transferable than a functional with *more* parameters. Consequently, additional empirical

parameters should be included in the functional form only if they contribute to improving the performance of the functional on *both* the training and primary test sets.

The first systematic optimization of a density functional[4] was conducted by Axel Becke in 1997. The resulting global hybrid (GH) GGA density functional, B97, had 10 linear parameters that resulted from uniformly truncating the power series ICFs for the exchange, same-spin correlation, and opposite-spin correlation functionals at second order ($m = 2$). Furthermore, Becke demonstrated that including more parameters into the linear fit negligibly enhanced the training set RMSD *and* introduced unphysically oscillatory character into the ICF plots.[4]

Becke revolutionized the systematic parameterization of exchange-correlation functionals with B97.[4] Since then, multiple B97-based density functionals have been developed. In 1998, Handy and coworkers[5] self-consistently optimized the parameters of Becke's functional (B97-1) and developed a new local GGA density functional (HCTH/93). With HCTH/93, the ICFs were truncated at $m = 4$ (for a total of 15 parameters) instead of at $m = 2$ as in the hybrid B97 and B97-1 functionals (10 parameters each). While Becke's work had indicated that values of $m > 2$ resulted in unphysical functionals, the use of $m = 4$ in HCTH/93 was justified by using a larger training set that included nuclear gradients and ZMP exchange-correlation potentials.[6] The same training procedure was used to develop 2 additional 15-parameter functionals (HCTH/120 and HCTH/147),[7] with the number following the slash indicative of the size of the training set. Handy's development of local GGA functionals culminated with the HCTH/407 functional[8] (15 parameters).

Additional attempts[9,10] at developing hybrid B97-based functionals were made by Tozer and coworkers with B97-2 and B97-3. B97-2 (10 parameters) kept the same value for m as B97 and B97-1, but included multiplicative potentials in its training set (following the example set by the HCTH family). Finally, B97-3 was parameterized with an even larger training set and an $m = 4$ truncation for the ICFs (16 parameters).

While the underlying ingredient that captures inhomogeneities in the density in B97-based density functionals is the gradient of the density, the first systematic optimization of a meta-GGA density functional was conducted almost simultaneously by Scuseria (VSXC)[11] and Becke (B98).[12] Both of these functionals were introduced nearly 10 years after Becke had first motivated the use of the kinetic energy density (and the Laplacian of the density) with the BR89 exchange functional[13] and the Bc88 correlation functional.[14] While the 10-parameter B98 functional included a fraction of exact exchange and depended on the density, the gradient and Laplacian of the density, as well as the kinetic energy density, the 21-parameter VSXC functional contained no exact-exchange mixing and depended on the density, its gradient, and the kinetic energy density.

Handy's entry into the world of meta-GGAs came with the B97- and B98-based τ-HCTH (16 parameters) and (global) hybrid τ-HCTH (17 parameters) functionals.[15] While the correlation functionals of both τ-HCTH and hybrid τ-HCTH were based on the B97 functional form, the exchange functionals had a B97-type component *and* a B98-type component (with a slightly modified τ-dependent dimensionless parameter (w_σ) introduced by Becke[16]).

In the spirit of non-empiricism, the meta-GGA counterpart of PBE, TPSS,[17] was developed in 2003, followed by the 17-parameter, global hybrid meta-GGA functional, BMK.[18] The functional form of BMK was virtually identical to that of the hybrid τ-HCTH functional, but a primary goal of its parameterization was improved performance for kinetics.

Since 2005, Truhlar has developed 10 highly-parameterized local (M06-L,[19] M11-L[20]), global hybrid (M05,[21] M05-2X,[22] M06,[23] M06-2X,[23] M06-HF,[24] M08-HX,[25] M08-SO[25]), and range-separated hybrid (M11[26]) meta-GGA density functionals with 20 to 50 parameters. The underlying parameterizable exchange functional component for the Minnesota functionals is a power series (in Becke's w_σ parameter) that multiplies the non-empirical GGA enhancement factor of the PBE exchange functional. Additional components for select functionals

include VSXC- and RPBE-based[27] exchange functional ICFs and PBE-, B97-, VSXC-, and B98-based correlation functional ICFs.

While attempts to remedy the self-interaction error (SIE) inherent to most density functionals date back to the early 1980s,[28] the elimination of SIE in the long-range (for the exchange functional) was facilitated by the development of range-separation, namely, the splitting of the Coulomb operator into short- and long-range components controlled by the erfc and erf functions, respectively. While this separation was initially used by Savin[29] to combine short-range DFT with long-range configuration-interaction, Hirao[30] successfully applied this scheme to Becke's B88 exchange functional[31] and combined it with his one-parameter progressive correlation functional[32,33] to produce LRC-BOP. In addition to eliminating long-range self-interaction for the exchange functional, range-separated hybrid functionals come with further benefits including improved performance for Rydberg and charge transfer excitations within the TD-DFT approach.[34]

While Hirao's approach to range separation involved using the analytic expression for the LSDA exchange hole[35] along with a modified Fermi wave vector that contained the exchange functional ICF to derive the expression for the range-separated enhancement factor for the LSDA exchange energy density, an alternate path[36–38] was pursued by Scuseria whereby a general model for the GGA exchange hole was developed and used to obtain the range-separated enhancement factor. Since the efforts of Scuseria[36–39] and Herbert[40,41] were directed towards combining the long-range-corrected (LRC) approach with existing exchange and correlation functionals, Chai and Head-Gordon used the flexible B97 functional form as the foundation for a series of semi-empirical, range-separated hybrid functionals, namely, ωB97,[42] ωB97X,[42] and ωB97X-D.[43] While the ICFs of these functionals were uniformly truncated at $m = 4$, the uniform electron gas (UEG) limits were satisfied, resulting in a total of 13, 14, and 15 optimized parameters, respectively. Furthermore, these functionals used the LRC scheme of Hirao rather than Scuseria.

Since long-range electron correlations that account for van der Waals (vdW) interactions cannot be properly described by standard density functionals,[44,45] there has been an increased effort in the past decade to remedy this issue. A comprehensive review of various approaches to extending the applicability of DFT to dispersive interactions can be found in Reference 46.

The simplest and cheapest methods that account for dispersion are Grimme's empirical DFT-D methods.[47–49] Grimme's first attempt at an empirical dispersion tail was DFT-D1,[47] which was only available for 6 elements (H, C, N, O, F, and Ne). With the atomic C_6 parameters and van der Waals Radii predetermined, the single linear optimizable parameter of the DFT-D1 dispersion tail (s_6) was trained onto 3 existing local GGA density functionals (BLYP, BP86, and PBE) and dramatically improved the ability of the parent functional to describe vdW interactions.

Following the success of DFT-D1, Grimme introduced the DFT-D2 dispersion tail along with an explicitly parameterized, B97-based, local GGA density functional called B97-D. B97-D maintained Becke's $m = 2$ truncation for the ICFs and had a total of 10 optimized parameters. While the form of the DFT-D2 dispersion correction term was identical to that of DFT-D1, atomic C_6 parameters and van der Waals Radii were made available for all elements through xenon, and the existing values from DFT-D1 were improved. Furthermore, s_6 parameters were determined for PBE, BLYP, BP86, TPSS, and B3LYP.

The latest addition to the DFT-D family is the DFT-D3 dispersion tail, which uses fractional coordination numbers to account for variations in atomic dispersion coefficients in different chemical environments and contains a 2-body *and* 3-body term. In addition, DFT-D3 uses an improved damping function (motivated by the work of Salahub[50] and Head-Gordon[43]) that has an additional nonlinear parameter in its denominator. Since the 2-body part of DFT-D3 includes both $1/r^6$ and $1/r^8$ terms, 2 linear (s_6 and s_8) and 2 nonlinear parameters ($s_{r,6}$

and $s_{r,8}$) are available for optimization. However, Grimme and coworkers demonstrated that s_6 and $s_{r,8}$ can be set to unity for non-double-hybrid density functionals, leaving 2 optimizable parameters. The DFT-D3 dispersion tail was trained onto more than 10 existing density functionals and generally improved upon its predecessors for describing dispersive interactions.

The Becke and Johnson (BJ) exchange-dipole moment (XDM) model[51–57] takes advantage of the fact that dispersive interactions can be accounted for via the exchange-hole dipole moments of the interacting species. The prominent term in such an (attractive) interaction is of the instantaneous dipole-induced dipole nature, and Becke and Johnson have motivated 2 variants of their method: XDM6, which only includes interatomic $1/r^6$ interactions, and XDM10, which additionally depends on interatomic $1/r^8$ and $1/r^{10}$ interactions. XDM6 and XDM10 have 1 and 2 optimizable parameters, respectively, and the methods have been recently implemented in both a self-consistent-field (SCF) and post-SCF manner.[58]

While the DFT-D and XDM approaches rely on predetermined atomic parameters (C_6 coefficients, vdW Radii, atomic polarizabilities, etc.) to compute the dispersion interaction, several methods that account for dispersion through their dependence on the electron density have been developed in the past decade, including vdW-DF-04,[59] vdW-DF-10,[60] VV09,[61] and VV10.[62] These nonlocal correlation (NLC) functionals rely on a double space integral over the density and a nonlocal correlation kernel, and are computationally more expensive than the DFT-D and XDM methods. Langreth, Lundqvist, and coworkers introduced the first NLC scheme (vdW-DF-04) that could be applied to overlapping densities in 2004. Several years later, Vydrov and Van Voorhis self-consistently implemented the vdW-DF-04 NLC functional for use with Gaussian basis sets,[63] and proposed modifications (vdW-DF-09) to improve its compatibility with existing exchange functionals.[64] The VV09[61,65,66] NLC functional of Vydrov and Van Voorhis adopted a simple analytic form for the nonlocal correlation kernel, instead of relying on numerical interpolation tables. Based on their experience garnered from VV09, Vydrov and Van Voorhis proposed an even simpler NLC functional, VV10, that improved upon its predecessor by employing a less elaborate function for the damping of the $1/r^6$ asymptote. In 2010, Langreth, Lundqvist, and coworkers proposed an improved NLC functional (vdW-DF-10) to account for the tendency of vdW-DF-04 to overestimate equilibrium bond lengths and underestimate the binding energies of hydrogen-bonded complexes. While the vdW-DF methods have no optimizable parameters, VV09 and VV10 have 1 and 2 optimizable parameters, respectively.

1.2 Design Goals and Strategy

Due to the flexibility provided by the B97 functional form, it is the foundation for the functional introduced in this paper. 3 significant changes are made to the original B97 functional form: 1). the new functional is a range-separated hybrid functional instead of a global hybrid functional, 2). the VV10 NLC functional[62] is included to provide a sound description of nonlocal electron correlation, and 3). the ICF truncation orders for the exchange, same-spin correlation, and opposite-spin correlation functionals are determined individually. The resulting density functional, ωB97X-V, has 7 linear parameters (2 for local exchange, 4 for local correlation, and 1 for short-range exact exchange) and 3 nonlinear parameters (1 for range-separation and 2 for nonlocal correlation), for a total of 10 optimized parameters.

The ingredients included in the functional form of ωB97X-V place it on the fourth rung of Perdew's "Jacob's Ladder"[67] (Figure 1). An alternate view of the ingredients that can be incorporated into a density functional is given in Table 1. When choosing the components of a density functional, the first consideration involves selecting the ingredients that will constitute the local exchange-correlation (xc) functional. While the density and its gradient were chosen for ωB97X-V, it is worthwhile to note that the kinetic energy density,

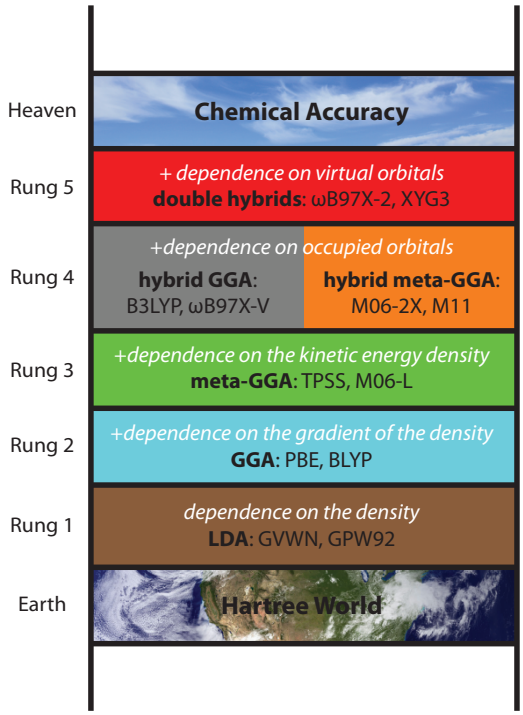

Figure 1: Perdew's "Jacob's Ladder".

$\tau_\sigma = \frac{1}{2}\sum_i^{occ.} |\nabla\psi_{i,\sigma}|^2$, was taken into consideration. However, studies[68–71] have indicated that functionals containing this ingredient require very fine integration grids to overcome oscillatory behavior in the potential energy curves (PEC) of weakly-bound systems. Furthermore, preliminary results from attempting to develop a range-separated hybrid meta-GGA density functional have indicated that the great freedom associated with parameterizing a $(\nabla\rho, \tau)$ surface requires further exploration, and will be addressed in a future publication.

After finalizing the local xc functional form, the question of whether to include exact exchange arises. Since most density functionals that perform well on both bonded and non-bonded interactions have a fraction of exact exchange, the subsequent question is whether to go with the global hybrid (GH) functional form or the range-separated hybrid (RSH) functional form. While GH functionals have a fixed fraction of exact exchange for all interelectronic distances, the fraction of exact exchange varies from 0 (or a positive non-zero fraction) at short-range to 1 at long-range for RSH functionals, conveniently eliminating self-interaction error in the long-range for the exchange functional. Since GH and RSH functionals have the same computational scaling, the RSH functional form was chosen for ωB97X-V.

Finally, it is necessary to decide whether a dispersion correction should be appended to the functional. Since a range-separated hybrid GGA functional cannot accurately bind dispersion-bound systems on its own, a nonlocal correlation correction is required. As a result of the poor performance of ωB97X-D on a recent benchmark of dianionic sulfate-water clusters[72] (a failure that can be attributed to the fact that dispersion tails cannot differentiate between neutral and charged atoms), the DFT-D methods were not considered. The NLC functional of Vydrov and Van Voorhis (VV10) was selected over MP2 because it does not carry the additional weight of fifth-order computational scaling and is a simple functional of the electron density. These considerations ultimately led to the functional form containing the underlined components in Table 1.

Table 1: Ingredients that can be incorporated into a density functional. GH stands for global hybrid and RSH stands for range-separated hybrid. The nonlocal correlation list is certainly not comprehensive, as it excludes functionals such as VV09, XDM6, XDM10, vDW-DF-04, and vDW-DF-10, as well as higher-scaling post-SCF methods like RPA, MP3, CCSD, and CCSD(T). The underlined ingredients define the functional form of ωB97X-V.

Exchange		Correlation	
Local	Nonlocal	Local	Nonlocal
1). $\underline{\rho}$	1). None	1). $\underline{\rho}$	1). None
2). $\underline{\nabla\rho}$	2). GH	2). $\underline{\nabla\rho}$	2). DFT-D2
3). $\underline{\tau}$	3). <u>RSH</u>	3). $\underline{\tau}$	3). DFT-D3
4). $\nabla^2\rho$		4). $\nabla^2\rho$	4). <u>VV10</u>
			5). MP2

The transferability of a semi-empirical density functional is an attribute that must be assured during its development. In order to obtain a maximally-transferable functional, the 2301 datapoints that were initially set aside for

training were divided into a training set of 1108 datapoints and a primary test set of 1193 datapoints. The motivation for this partitioning initially came from the decision to determine the 3 ICF expansions individually, instead of truncating them uniformly. During the optimization of B97, Becke uniformly varied the truncation order (m) from 0 to 8, and chose to truncate uniformly at $m = 2$ based on the 9 resulting RMSDs. In this work, the decision to individually determine the ICF expansions means that there are $2^{m_x+m_{css}+m_{cos}+2}-1$ possible candidate functionals (where m_x, m_{css}, and m_{cos} are the largest orders included in the exchange, same-spin correlation, and opposite-spin correlation functional power series ICFs). Since there is no literature on whether truncating the ICFs individually and/or skipping orders in the ICFs will produce transferable functionals, it was deemed necessary to train the linear parameters of the candidate functionals on the training set and check the transferability of the fits on the primary test set. Ultimately, this survival-of-the-fittest strategy will be used to answer the following basic questions: 1). "Does having more parameters necessarily imply better overall performance for a density functional?", 2). "Is there a point at which the inclusion of additional parameters becomes detrimental to the overall performance of a density functional?", and 3). "Can we achieve better overall performance by selectively optimizing certain parameters in the ICFs, or is the conventional scheme of uniform truncation better?".

2 Computational Details

An integration grid of 99 radial points and 590 angular points, (99,590), was used to evaluate local xc functionals, while the SG-1 grid[73] was used for the VV10 NLC functional.[62] For the rare-gas dimers and the absolute atomic energies, a (500,974) integration grid was used to evaluate local xc functionals, along with a (99,590) grid for the VV10 NLC functional. For M06-L[19] and M11-L,[20] calculations in the training and primary test set were carried out with the (250,590) grid. All calculations on the coronene dimer were carried out with a (75,302) grid for local xc functionals and SG-1 for the VV10 NLC functional. The aug-cc-pVQZ [aQZ] basis set[74,75] was used for all thermochemistry datapoints except the second-row absolute atomic energies (aug-cc-pCVQZ),[74,75] while the aug-cc-pVTZ [aTZ] basis set[74,75] was used for all noncovalent interactions datapoints except the rare-gas dimers (aug-cc-pVQZ). For the X40 dataset[76] in the secondary test set, the def2-TZVPPD basis set[77,78] was used. Furthermore, the noncovalent interactions were computed *without* counterpoise corrections unless otherwise noted. For PBE-D2, B3LYP-D2, and B97-D2, Grimme's DFT-D2 dispersion tail was used with the following[48,79] s_6 coefficients: 0.75, 1.05, and 0.75. Grimme's B97-D functional uses the DFT-D2 dispersion tail as well, with an s_6 coefficient of 1.25. All of the calculations were performed with a development version of Q-Chem 4.0.[80]

3 Theory

The complete functional form for ωB97X-V is given by Equations 1-3. The components of the exchange functional and correlation functional are described in Sections 3.1 and 3.2, respectively. The acronyms used in Equations 1-3 (and henceforth) are: exchange-correlation (xc), exchange (x), correlation (c), short-range (sr), long-range (lr), same-spin (ss), opposite-spin (os), and nonlocal (nl).

$$E_{xc}^{\omega B97X-V} = E_{x}^{\omega B97X-V} + E_{c}^{\omega B97X-V} \quad (1)$$

$$E_{x}^{\omega B97X-V} = E_{x,sr}^{B97} + c_x E_{x,sr}^{exact} + E_{x,lr}^{exact} \quad (2)$$

$$E_{c}^{\omega B97X-V} = E_{c,ss}^{B97} + E_{c,os}^{B97} + E_{c,nl}^{VV10} \quad (3)$$

3.1 Exchange Functional Form

The local spin-density approximation (LSDA) for exchange can be expressed in terms of the first-order spinless reduced density matrix for a uniform electron gas (UEG):

$$E_x^{LSDA} = -\frac{1}{2}\sum_{\sigma}^{\alpha,\beta}\int\int \frac{1}{s}|\rho_{\sigma}^{UEG}(\mathbf{r},s)|^2 d\mathbf{r}d\mathbf{s} \quad (4)$$

$$\rho_{\sigma}^{UEG}(\mathbf{r},s)=3\rho_{\sigma}(\mathbf{r})\left[\frac{\sin(k_{F\sigma}s)-k_{F\sigma}s\cos(k_{F\sigma}s)}{[k_{F\sigma}s]^{3}}\right] \tag{5}$$

where $\mathbf{s}=\mathbf{r}_1-\mathbf{r}_2$, $\mathbf{r}=\frac{1}{2}[\mathbf{r}_1+\mathbf{r}_2]$, and $k_{F\sigma}=[6\pi^2\rho_{\sigma}]^{1/3}$ is the spin-polarized Fermi wave vector. Integration of Equation 4 over $\mathbf{s}$ gives the well-known expression for the LSDA exchange energy in terms of the exchange energy density per unit volume of a uniform electron gas:

$$E_x^{LSDA}=\sum_{\sigma}^{\alpha,\beta}\int e_{x,\sigma}^{UEG}(\rho_{\sigma})d\mathbf{r} \tag{6}$$

$$e_{x,\sigma}^{UEG}(\rho_{\sigma})=-\frac{3}{2}\left(\frac{3}{4\pi}\right)^{1/3}\rho_{\sigma}^{4/3} \tag{7}$$

Transforming E_x^{LSDA} to its short-range counterpart, $E_{x,sr}^{LSDA}$, is accomplished by replacing $\frac{1}{s}$ in Equation 4 with $\frac{\mathrm{erfc}(\omega s)}{s}$ and carrying out the same integration. The resulting SR-LSDA exchange functional:

$$E_{x,sr}^{LSDA}=\sum_{\sigma}^{\alpha,\beta}\int e_{x,\sigma}^{UEG}(\rho_{\sigma})F(a_{\sigma})\,d\mathbf{r} \tag{8}$$

is conveniently identical to its unattenuated counterpart, with the exception of a multiplicative attenuation function, $F(a_\sigma)$:

$$F(a_{\sigma})=1-\frac{2}{3}a_{\sigma}\left[2\sqrt{\pi}\mathrm{erf}\left(\frac{1}{a_{\sigma}}\right)-3a_{\sigma}+a_{\sigma}^{3}+\left[2a_{\sigma}-a_{\sigma}^{3}\right]\exp\left(-\frac{1}{a_{\sigma}^{2}}\right)\right] \tag{9}$$

where $a_\sigma=\frac{\omega}{k_{F\sigma}}$ and ω is the nonlinear range-separation parameter that controls the transition from local DFT exchange to nonlocal exact exchange with respect to interelectronic distance.

Accounting for inhomogeneities in the electron density is achieved by multiplying the integrand of the SR-LSDA exchange functional by the power series inhomogeneity correction factor,[4] $g_x(u_{x,\sigma})$, resulting in the SR-B97 exchange functional:

$$E_{x,sr}^{B97}=\sum_{\sigma}^{\alpha,\beta}\int e_{x,\sigma}^{UEG}(\rho_{\sigma})F(a_{\sigma})\,g_x(u_{x,\sigma})\,d\mathbf{r} \tag{10}$$

$$g_x(u_{x,\sigma})=\sum_{i=0}^{m_x}c_{x,i}u_{x,\sigma}^{i}=\sum_{i=0}^{m_x}c_{x,i}\left[\frac{\gamma_x s_{\sigma}^2}{1+\gamma_x s_{\sigma}^2}\right]^{i} \tag{11}$$

where the dimensionless variable, $u_{x,\sigma}\in[0,1]$, is a finite domain transformation of the reduced spin-density gradient, $s_\sigma=\frac{|\nabla\rho_\sigma|}{\rho_\sigma^{4/3}}\in[0,\infty)$. The linear DFT exchange parameters, $c_{x,i}$, will be determined by least-squares fitting to a training set in Section 5, while $\gamma_x=0.004$ is a nonlinear DFT exchange parameter that was fit to the Hartree–Fock exchange energies of 20 atoms in 1986 by Becke.[81]

Nonlocal exchange is introduced by splitting the Coulomb operator in the conventional expression for exact exchange into a short-range component ($E_{x,sr}^{exact}$) and a long-range component ($E_{x,lr}^{exact}$) with the erfc and erf Coulomb functions, respectively:

$$E_{x,sr}^{exact}=-\frac{1}{2}\sum_{\sigma}^{\alpha,\beta}\sum_{i,j}^{occ.}\int\int\psi_{i\sigma}^{*}(\mathbf{r}_1)\,\psi_{j\sigma}^{*}(\mathbf{r}_2)\,\frac{\mathrm{erfc}(\omega r_{12})}{r_{12}}\times\psi_{j\sigma}(\mathbf{r}_1)\,\psi_{i\sigma}(\mathbf{r}_2)\,d\mathbf{r}_1 d\mathbf{r}_2 \tag{12}$$

$$E_{x,lr}^{exact}=-\frac{1}{2}\sum_{\sigma}^{\alpha,\beta}\sum_{i,j}^{occ.}\int\int\psi_{i\sigma}^{*}(\mathbf{r}_1)\,\psi_{j\sigma}^{*}(\mathbf{r}_2)\,\frac{\mathrm{erf}(\omega r_{12})}{r_{12}}\times\psi_{j\sigma}(\mathbf{r}_1)\,\psi_{i\sigma}(\mathbf{r}_2)\,d\mathbf{r}_1 d\mathbf{r}_2 \tag{13}$$

where $\psi_{i\sigma}$ and $\psi_{j\sigma}$ are the occupied Kohn–Sham spatial orbitals. Instead of setting the percentage of exact-exchange at $r=0$ to zero, an optimizable parameter, c_x, controls the amount of short-range exact exchange.

3.2 Correlation Functional Form

Closed-form expressions for the correlation energy density per particle of a uniform electron gas, $\epsilon_c^{UEG}(\rho)$, are only known for the low- and high-density limits of the paramagnetic and ferromagnetic cases of the uniform electron gas (UEG). Using the Monte-Carlo data of Ceperley and Alder,[82] Perdew and Wang developed an analytical spin-compensated representation,[83] $\epsilon_c^{PW92}(\rho)$, for $\epsilon_c^{UEG}(\rho)$. Combined with the spin-polarization interpolation formula of Vosko, Wilk, and Nusair,[84] the spin-polarized PW92 correlation energy density per particle, $\epsilon_c^{PW92}(\rho_\alpha,\rho_\beta)$, is the starting point for the ωB97X-V correlation functional:

$$E_c^{LSDA} = \int \rho \epsilon_c^{PW92}\left(\rho_\alpha, \rho_\beta\right) d\mathbf{r} \tag{14}$$

Using the spin decomposition technique of Hermann Stoll and coworkers,[85] the LSDA correlation energy functional above can be separated into same-spin and opposite-spin components:

$$E_{c,ss}^{LSDA} = \sum_{\sigma}^{\alpha,\beta} \int e_{c,\sigma\sigma}^{PW92} d\mathbf{r} = \int \rho_\alpha \epsilon_c^{PW92}\left(\rho_\alpha, 0\right) d\mathbf{r} + \int \rho_\beta \epsilon_c^{PW92}\left(0, \rho_\beta\right) d\mathbf{r} \tag{15}$$

$$E_{c,os}^{LSDA} = \int e_{c,\alpha\beta}^{PW92} d\mathbf{r} = \int \rho \epsilon_c^{PW92}\left(\rho_\alpha, \rho_\beta\right) d\mathbf{r} - \int \rho_\alpha \epsilon_c^{PW92}\left(\rho_\alpha, 0\right) d\mathbf{r} - \int \rho_\beta \epsilon_c^{PW92}\left(0, \rho_\beta\right) d\mathbf{r} \tag{16}$$

where $e_{c,\sigma\sigma}^{PW92}$ and $e_{c,\alpha\beta}^{PW92}$ are the PW92 same-spin and opposite-spin correlation energy densities per unit volume. Extending Equations 15 and 16 to account for inhomogeneities in the electron density is straightforward, since the same approach used for the exchange functional can be applied to the correlation functional:

$$E_{c,ss}^{B97} = \sum_{\sigma}^{\alpha,\beta} \int e_{c,\sigma\sigma}^{PW92} g_{c,ss}\left(u_{c,\sigma\sigma}\right) d\mathbf{r} \tag{17}$$

$$g_{c,ss}\left(u_{c,\sigma\sigma}\right) = \sum_{i=0}^{m_{css}} c_{css,i} u_{c,\sigma\sigma}^i = \sum_{i=0}^{m_{css}} c_{css,i} \left[\frac{\gamma_{css} s_\sigma^2}{1 + \gamma_{css} s_\sigma^2}\right]^i \tag{18}$$

$$E_{c,os}^{B97} = \int e_{c,\alpha\beta}^{PW92} g_{c,os}\left(u_{c,\alpha\beta}\right) d\mathbf{r} \tag{19}$$

$$g_{c,os}\left(u_{c,\alpha\beta}\right) = \sum_{i=0}^{m_{cos}} c_{cos,i} u_{c,\alpha\beta}^i = \sum_{i=0}^{m_{cos}} c_{cos,i} \left[\frac{\gamma_{cos} s_{\alpha\beta}^2}{1 + \gamma_{cos} s_{\alpha\beta}^2}\right]^i \tag{20}$$

where $s_{\alpha\beta}^2 = \frac{1}{2}\left(s_\alpha^2 + s_\beta^2\right)$. The linear DFT correlation parameters, $c_{css,i}$ and $c_{cos,i}$, will be determined by least-squares fitting to a training set in Section 5, while $\gamma_{css} = 0.2$ and $\gamma_{cos} = 0.006$ are nonlinear DFT correlation parameters that were fit to the correlation energies of helium and neon in 1986 by Becke.[81]

Nonlocal correlation is taken into account via the VV10 NLC functional:[62]

$$E_{c,nl}^{VV10} = \int \rho\left(\mathbf{r}\right) \left[\frac{1}{32}\left[\frac{3}{b^2}\right]^{3/4} + \frac{1}{2}\int \rho\left(\mathbf{r}'\right) \Phi\left(\mathbf{r}, \mathbf{r}', \{b, C\}\right) d\mathbf{r}'\right] d\mathbf{r} \tag{21}$$

where $\Phi\left(\mathbf{r}, \mathbf{r}', \{b, C\}\right)$ is the nonlocal correlation kernel defined in Reference 62. The VV10 NLC functional introduces 2 nonlinear parameters: b, which controls the short-range damping of the R^{-6} asymptote, and C, which controls the accuracy of the asymptotic C_6 coefficients.

4 Datasets

In total, the training, primary test, and secondary test sets used for the parameterization, validation, and assessment of ωB97X-V contain 2486 datapoints, requiring 2455 single-point calculations. Of the 2486 datapoints, 1108 belong to the training set, 1193 belong to the primary test set, and 185 belong to the secondary test set. Furthermore, the training, primary test, and secondary test sets contain both thermochemistry (TC) data as well as noncovalent interactions (NC) data. The training set contains 787 TC datapoints and 321 NC datapoints, the primary test set contains 146 TC datapoints and 1047 NC datapoints, and the secondary test set contains 69 TC datapoints and 116 NC datapoints (for an overall total of 1002 TC datapoints and 1484 NC datapoints). Table 2 lists the 47 datasets that form the training, primary test, and secondary test sets. Details regarding the datasets will be discussed in this section. The references for the datasets are given in the rightmost column of Table 2 and will not be repeated in the text unless specific values from a table are being referenced.

The first 5 thermochemistry datasets in the training set are from Jan Martin's W4-11 dataset. All datapoints that involve multireference systems were removed from these datasets.

The reference values for DBH24 were taken from the second column ("TAE_e") of Table 1 in Reference 86 and the geometries were taken from the online Minnesota databases.

EA6 and EA7 (as well as IP6 and IP7) are subsets of Truhlar's EA13 and IP13 datasets. For the atoms in EA6 and IP6 (C, O, Si, P, S,

and Cl), the reference values were recomputed at the CCSD(T)/aug-cc-pwC(Q5)Z[75,118] level, while for the remaining molecules in EA7 and IP7, the 14 reference values (as well as the geometries) were taken from the online Minnesota databases (Column "REF1" in EA13/03 and IP21).

AE8 contains the absolute energies of the following atoms: H, He, B, C, N, O, F, and Ne. The energies for the latter 6 atoms were taken from Table XI (rightmost entry) in Reference 87, while the exact energies of the hydrogen atom (-0.5 hartree) and the helium atom[119] (-2.90372 hartrees) were used.

Moving on to the NC data in the training set, 3 potential energy curves (PEC) were removed from Sherrill's NBC10A dataset (parallel-displaced benzene dimer (3.2 Å and 3.6 Å) and benzene-H_2S dimer), and the rest of the PECs were divided into 3 subdatasets (NBC10A1, NBC10A2, and NBC10A3), while all 6 PECs from HBC6A were used.

From Crittenden's BzDC215 dataset, the following interactions were included in the training set: C_6H_6-{HF, H_2O, NH_3, CH_4, HCl}.

The reference values for AlkAtom19, AlkIsomer11, and AlkIsod14 were taken from Tables S7, S8, and S9 of the Supporting Information of Reference 88 (along with the B3LYP/pc-2 optimized geometries).

The geometries and reference values for HTBH38 and NHTBH38 were taken from the online Minnesota databases (Column "REF1" in HTBH38/08 and NHTBH38/08).

For the rare-gas dimers, the PECs each have 41 points with the following ranges in increments of 0.1 Å: Ne_2 (2.59 to 6.59 Å), Ar_2 (3.26 to 7.26 Å), and NeAr (2.98 to 6.98 Å). The reference values were taken from the Tang-Toennies potential model.

From WATER27, the 4 datapoints corresponding to the water 20-mers were excluded, and the rest of the reference values and geometries were taken from Grimme's online GMTKN30 database.

For HW30, the reference values were taken from the fourth column ("$E_{int}^{CCSD(T)/CBS}$") of Table 1 in Reference 89.

For NCCE31, only the 18 interactions from Table 1 of Reference 90 were used, and the reference values in the last column ("final D_e") of this table were used. The geometries were taken from the online Minnesota databases.

The revised S22B values from Sherrill were used for the S22 dataset, while Hobza's revised S66 reference values were used for the S66 dataset.

The reference values and geometries for G21EA, G21IP, and CYCONF were taken from Grimme's online GMTKN30 database. The reference values and geometries for PA8 were taken from the online Minnesota databases (Column "REF1" in PA8/06). For A24, the reference values were computed by adding the values in the "CCSD(T)/CBS" and "core correlation" columns in Table 1 of Reference 108.

The MP2/haTZ optimized geometries for the 8 water hexamers (bag, book1, book2, cage, cyclicboat1, cyclicboat2, cyclicchair (ring), prism) in H2O6Rel and H2O6Bind were taken from References 106 and 107. The term, haTZ, indicates that the aug-cc-pVTZ basis set was used for oxygen and the cc-pVTZ basis set was used for hydrogen. The binding energies in H2O6Bind were taken from the last column ("CCSD(T)/CBS - relaxation") of Table S5 in the Supporting Information of Reference 91, and the relative energies in H2O6Rel were computed using the binding energies in H2O6Bind (i.e. not the hexamer absolute energies).

The reference values for HW6F and HW6Cl were taken from the third column ("RI-CCSD(T)/CBS") of Tables S6 and S7 in the Supporting Information of Reference 91.

The reference values for DS14 were taken from the third column ("CBS (ΔaTZ)") of Table 1 in Reference 109.

5 Training

With a training set of 1108 datapoints, it is clear that a comprehensive 3-parameter nonlinear optimization is impractical. As a result, the 3 nonlinear parameters were determined from fits to a subset of the training set over a 3-dimensional set of points. The resulting values for ω, b, and C were 0.3, 6.0, and 0.01,

Table 2: Summary of the datasets found in the training, primary test, and secondary test sets. The datasets above the first thick black line are in the training set, the datasets between the first and second thick black lines are in the primary test set, while the datasets below the second thick black line are in the secondary test set. Within the training, primary test, and secondary test sets, datasets above the thin black line contain thermochemistry datapoints, while datasets below the thin black line contain noncovalent interactions datapoints. PEC stands for potential energy curve.

Name	Description	#	Ref.
HAT707	Heavy-atom transfer reaction energies	505	104
BDE99	Bond dissociation reaction energies	83	104
TAE_nonMR124	Total atomization energies	124	104
SN13	Nucleophilic substitution reaction energies	13	104
ISOMER20	Isomerization reaction energies	18	104
DBH24	Diverse barrier heights	24	86,92
EA6	Electron affinities of atoms	6	103
IP6	Ionization potentials of atoms	6	103
AE8	Absolute atomic energies	8	87
SW49Rel345	$SO_4{}^{2-}(H_2O)_n$ ($n = 3-5$) relative energies	28	72
SW49Bind345	$SO_4{}^{2-}(H_2O)_n$ ($n = 3-5$) binding energies	30	72
NBC10A2	Methane dimer and benzene-methane dimer PECs	37	102,115
HBC6A	Formic acid, formamide acid, and formamidine acid dimer PECs	118	100,115
BzDC215	Benzene and first- and second-row hydride PECs	108	117
EA7	Electron affinities of small molecules	7	103
IP7	Ionization potentials of small molecules	7	103
Gill12	Neutral, radical, anionic, and cationic isodesmic reaction energies	12	93
AlkAtom19	$n = 1-8$ alkane atomization energies	19	88
AlkIsomer11	$n = 4-8$ alkane isomerization energies	11	88
AlkIsod14	$n = 3-8$ alkane isodesmic reaction energies	14	88
HTBH38	Hydrogen transfer barrier heights	38	94
NHTBH38	Non-hydrogen transfer barrier heights	38	95
SW49Rel6	$SO_4{}^{2-}(H_2O)_n$ ($n = 6$) relative energies	17	72
SW49Bind6	$SO_4{}^{2-}(H_2O)_n$ ($n = 6$) binding energies	18	72
NNTT41	Neon-neon PEC	41	116
AATT41	Argon-argon PEC	41	116
NATT41	Neon-argon PEC	41	116
NBC10A1	Parallel-displaced (3.4 Å), sandwich, and T-shaped benzene dimer PECs	53	102,115
NBC10A3	S2 and T3 configuration pyridine dimer PECs	39	101,115
WATER27	Neutral and charged water interactions	23	110,111
HW30	Hydrocarbon and water dimers	30	89
NCCE31	Noncovalent complexation energies	18	90
S22x5	Hydrogen-bonded and dispersion-bonded complex PECs	110	96
S66x8	Biomolecular structure complex PECs	528	113
S22	Equilibrium geometries from S22x5	22	112,115
S66	Equilibrium geometries from S66x8	66	113,114
G21EA	Adiabatic electron affinities	25	105,111
G21IP	Adiabatic ionization potentials	36	105,111
PA8	Adiabatic proton affinities	8	97,98
A24	Small noncovalent complexes	24	108
X40	Noncovalent interactions of halogenated molecules	40	76
H2O6Rel	Relative energies of water hexamers	8	91
H2O6Bind	Binding energies of water hexamers	8	91
HW6F	Binding energies of $F^-(H_2O)_n$ ($n = 1-6$)	6	91
HW6Cl	Binding energies of $Cl^-(H_2O)_n$ ($n = 1-6$)	6	91
CYCONF	Relative energies of cysteine conformers	10	99,111
DS14	Binding energies for complexes containing divalent sulfur	14	109

respectively. ω was optimized in increments of 0.1, b was optimized in increments of 0.25, and C was optimized in increments of 0.0025. In comparison to existing functionals, the value of $\omega = 0.3$ is identical to the value that was determined for ωB97X[42] by Chai and Head-Gordon. In addition, Vydrov and Van Voorhis[62] found that the best b and C values were 5.9 and 0.0093 for rPW86+PBE+VV10 [VV10] and 6.3 and 0.0089 for ωPBE+PBE+VV10 [LC-VV10]. Thus, the nonlinear values that have been determined are reasonable. Any inaccuracies in these parameters will be accounted for during the optimization of the linear parameters.

With the nonlinear parameters determined, the 1961 required single-point calculations (corresponding to the data in the training and primary test sets) were carried out with the unoptimized ωB97X-V functional ($g_x = g_{c,ss} = g_{c,os} = 1$) in order to acquire the data necessary to perform least-squares fits to the training set *and* check the accuracy of the fits on the primary test set. Contributions to the total energy from $u^i_{x,\sigma}$, $u^i_{c,\sigma\sigma}$, and $u^i_{c,\alpha\beta}$ for $i \in [0, 4]$ were saved, along with the contribution from $E^{exact}_{x,sr}$.

The only constraint that was deliberately enforced was the uniform electron gas limit for exchange ($c_{x,0} + c_x = 1$), since a review of the parameters of existing density functionals indicated that relaxing this constraint usually results in $c_{x,0} + c_x \approx 1$. For example, for B97,[4] $c_{x,0} + c_x = 1.0037$, and for B97-1,[5] $c_{x,0} + c_x = 0.999518$. On the other hand, $\{c_{ss,0},\ c_{os,0}\}$ for B97 and B97-1 are $\{0.17, 0.95\}$ and $\{0.08, 0.96\}$, respectively. Furthermore, since past experience with ωB97X[42] and ωB97X-D[43] indicated that c_x optimizes to a non-zero value (0.158 and 0.222, respectively), this parameter was always included in the least-squares fits.

With 4 free parameters from the exchange functional ICF, and 5 free parameters from each of the correlation functional ICFs, the total number of least-squares fits amounts to $\sum_{i=1}^{14} \binom{14}{i} = 2^{14} - 1 = 16383$.

Thermochemistry datapoints in the training and primary test sets are given weights of 1 and 2.5 respectively (except for datapoints in EA6 and IP6 which are weighted by 5), noncovalent interactions datapoints in the training and primary test sets are given weights of 10 and 25, respectively, and datapoints corresponding to the rare-gas dimer PECs in the primary test set are given weights of 25000. The total RMSD is defined as a weighted RMSD of all 1961 datapoints in the training and primary test sets, with the aforementioned weights.

Using the least-squares fits data, preliminary training set, primary test set, and total RMSDs were generated for all 16383 possible functional forms. Based on this data, it was concluded that fits that skip powers in the dimensionless variable, u, tend to perform comparably or worse than functionals with the same number of parameters that do not skip powers in u. After disregarding functionals that skip powers in u, a total of 500 unique functional forms remained.

The training set and primary test set RMSDs for these 500 least-squares fits plotted with respect to the number of linear parameters are shown in Figure 2. The data contained in Figure 2 is crucial for assessing the extent to which our design goal of a highly-accurate, transferable functional can be accomplished with minimal empiricism. Considering the figure on the left (which contains the training set RMSDs), it is evident that the best functional with a given number of linear parameters improves rapidly with each additional parameter up to 6 or 7 parameters. Subsequent additional parameters provide only small improvements to the training set RMSD. Thus, the curve corresponding to the lowest training set RMSD for a given number of linear parameters resembles a hockey stick.

On the right side of Figure 2 is the corresponding data for the primary test set RMSD. The most important attribute of this plot is that the curve defined by the lowest primary test set RMSD for a given number of linear parameters looks roughly similar to the plot on the left for up to 7 parameters, but the addition of more parameters leads to no improvement. In fact, the optimal primary test set RMSD values for functionals with more than 7 linear parameters gradually worsen, indicating reduced transferability. This plot depicts a

useful guideline for determining the appropriate "extent of empiricism".

In order to easily identify the functionals in Figure 2, the following nomenclature will be utilized: 3 numbers (0-4) will indicate at which order the exchange, same-spin correlation, and opposite-spin correlation functional ICFs are truncated, while 3 letters (y(es) or n(o)) will indicate whether or not the UEG limit is enforced. For example, 3y0n2n indicates that the exchange functional ICF is truncated at $m_x = 3$, while the same-spin and opposite-spin correlation functional ICFs are truncated at $m_{css} = 0$ and $m_{cos} = 2$, respectively. Furthermore, it indicates that the UEG limit for exchange is satisfied (by construction), while neither of the UEG limits for correlation are enforced.

The primary test set RMSD plot on the right in Figure 2 was used to identify outstanding functionals. This figure clearly indicates that increasing the number of linear parameters past 7 is either ineffective or detrimental towards the goal of minimizing the primary test set RMSD. The 2 7-parameter fits that have virtually the same primary test set RMSDs are: 2y1n1n (green square, gray check mark, 2.05 kcal/mol) and 2y2y1n (orange downright triangle, magenta check mark, 2.03 kcal/mol). In order to differentiate between the two, it was necessary to consider their performance on the training set as well. Accordingly, the training set RMSD plot on the left in Figure 2 indicates that the 2y1n1n functional (3.36 kcal/mol) has a slightly lower training set RMSD than the 2y2y1n functional (3.40 kcal/mol). To isolate the winner, the total RMSD was plotted in the same manner. Figure 3 shows the total RMSD for all 16383 least-squares fits and it is clear that the 2y1n1n functional is the optimal choice, even when functionals that skip orders in u are considered. Ultimately, the 2y1n1n functional with 7 linear parameters was selected for self-consistent optimization.

With a training set RMSD of 3.36 kcal/mol, a primary test set RMSD of 2.05 kcal/mol, and a total RMSD of 2.76 kcal/mol, the 2y1n1n functional compares very well to the "best" functional from each RMSD category. The functional with the lowest training set RMSD is the 15-parameter 4y4n4n functional at 3.16 kcal/mol (with a primary test RMSD of 15.57 kcal/mol and a total RMSD of 11.42 kcal/mol), while the functional with the lowest primary test set RMSD is the aforementioned 2y2y1n functional at 2.03 kcal/mol (with a total RMSD of 2.78 kcal/mol). Finally, the functional with the lowest total RMSD is the 8-parameter 2y2n1n functional. The 3 RMSDs of this fit match those of the 2y1n1n functional to the second decimal place, and the additional parameter is therefore unwarranted. Since Figure 3 plots the total RMSD for all 16383 fits, there are functional forms that skip orders in u that have slightly smaller total RMSDs than the 2y1n1n functional. The lowest total RMSD of 2.74 kcal/mol is achieved by a 9-parameter 2y4n1n functional that skips the first order linear parameter in $u_{c,\sigma\sigma}$. This fit has a training RMSD of 3.36 kcal/mol and a primary test set RMSD of 2.01 kcal/mol. However, its negligible improvement over the 2y1n1n functional form is not worth the 2 additional empirical parameters. Compared to the existing ωB97X and ωB97X-D functionals (13 linear parameters each), the new functional has 6 fewer linear parameters.

The training set RMSD of the unoptimized ωB97X-V functional is 25.84 kcal/mol, while the training set RMSD of the carefully selected 2y1n1n functional is 3.36 kcal/mol. With the data from Cycle 1, it is straightforward to produce a series of interesting results that will be discussed here. For example, if only the first-order gradient correction to the exchange functional is optimized (the resulting functional would be an RSH ($c_x = 0$) B86-type exchange functional with PW92 local correlation and VV10 nonlocal correlation), the resulting coefficient is $c_{x,1} = 0.718$. While it is not an apples-to-apples comparison, the corresponding coefficient that Becke determined in 1986 for the local B86 exchange-only functional by fitting to atomic exchange energies was 0.967. This single-parameter fit cuts the training set RMSD by more than a factor of 3 (7.76 kcal/mol). If only the short-range exact exchange parameter is allowed to vary (with the

UEG limit for exchange enforced), the resulting value is $c_x = 0.475$, with a training set RMSD of 10.47 kcal/mol. Finally, the training set RMSD for the 2n2n2n "B97" functional form is 3.34 kcal/mol, with a primary test set RMSD of 2.62 kcal/mol and a total RMSD of 2.99 kcal/mol. For comparison, the training set, primary test set, and total RMSDs for Becke's B97 functional are 4.36, 15.75, and 11.74 kcal/mol, respectively, while appending Grimme's DFT-D2 dispersion tail to B97 gives the resulting B97-D2 functional corresponding RMSDs of 3.36, 4.52, and 4.00 kcal/mol, respectively.

Including the initial cycle (Cycle 1) with the unoptimized ωB97X-V functional, the self-consistent optimization of ωB97X-V required 3 cycles. For the first cycle, the datapoints in the training *and* primary test sets were evaluated in order to generate Figures 2 and 3 and determine the functional form that would be self-consistently optimized. For the latter 2 cycles, only the 1108 datapoints in the training set were required to fine-tune the parameters. The parameters from the beginning of all 3 cycles are listed in Table 3.

The RMSDs for the 14 datasets in the training set are shown in Table 4. The columns labeled "Cycle 1" and "Cycle 3" contain the actual RMSDs from the end of the respective cycle, while the column labeled "Cycle 1P" contains the least-squares fit RMSDs from the end of the first cycle. Figures 2 and 3 were generated with the same data that is used to produce the values in the "Cycle 1P" column. It is quite remarkable that the least-squares fit RMSDs from Cycle 1P so closely resemble the final RMSDs of the ωB97X-V functional from Cycle 3. For all of the datasets except AE8, the least-squares fit and final RMSDs differ by 0.05 kcal/mol at most, while for AE8 the difference is 0.20 kcal/mol, due to the large magnitude of the absolute atomic energies.

6 Characteristics of ωB97X-V

The final parameters of ωB97X-V can be found in the fourth column of Table 3 under the "Cy-

Table 3: Linear parameters from the beginning of all 3 cycles of the self-consistent optimization of ωB97X-V. The corresponding nonlinear parameters are $\omega = 0.3$, $b = 6.0$, and $C = 0.01$. The final parameters are listed under Cycle 3. The value of $c_{x,0}$ is not listed because the uniform electron gas limit for exchange was enforced, requiring $c_{x,0} = 1 - c_x$. The initial guess ("Cycle 1") corresponding to the unoptimized ωB97X-V functional was attained by setting all of the linear parameters to zero, besides $c_{x,0} = c_{ss,0} = c_{os,0} = 1$.

Parameter	Cycle 1	Cycle 2	Cycle 3
$c_{x,1}$	1.000	0.614	**0.603**
$c_{x,2}$	0.000	1.181	**1.194**
$c_{ss,0}$	1.000	0.575	**0.556**
$c_{ss,1}$	0.000	-0.274	**-0.257**
$c_{ab,0}$	1.000	1.219	**1.219**
$c_{ab,1}$	0.000	-1.867	**-1.850**
c_x	0.000	0.163	**0.167**

Table 4: Training set RMSDs in kcal/mol for the 14 datasets comprising the training set. The columns labeled "Cycle 1" and "Cycle 3" contain the actual RMSDs from the end of the respective cycle, while the column labeled "Cycle 1P" contains the least-squares fit RMSDs from the end of the first cycle.

Dataset	Cycle 1	Cycle 1P	Cycle 3
HAT707	8.88	4.26	4.28
BDE99	15.10	3.36	3.38
TAE_nonMR124	36.14	3.31	3.34
SN13	11.48	0.97	1.01
ISOMER20	2.98	1.59	1.64
DBH24	7.56	1.77	1.81
EA6	12.42	2.35	2.34
IP6	12.54	3.74	3.76
AE8	247.87	1.57	1.77
SW49Rel345	1.49	0.34	0.33
SW49Bind345	4.22	0.31	0.29
NBC10A2	0.08	0.08	0.09
HBC6A	2.71	0.39	0.39
BzDC215	0.53	0.26	0.27

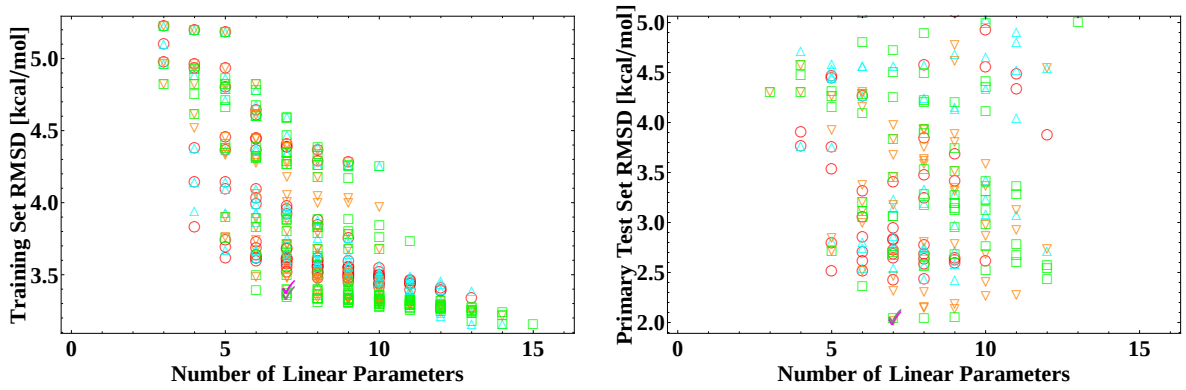

Figure 2: Training and primary test set RMSDs from 500 least-squares fits plotted against the number of linear parameters. Red circles indicate functionals that satisfy the UEG limits for exchange and correlation, upright cyan triangles indicate functionals that satisfy the UEG limits for exchange and opposite-spin correlation, downright orange triangles indicate functionals that satisfy the UEG limits for exchange and same-spin correlation, and green squares indicate functionals that satisfy the UEG limit for exchange only. The 2 checkmarked functionals are: 2y1n1n (gray) and 2y2y1n (magenta). The nomenclature is explained in Section 5.

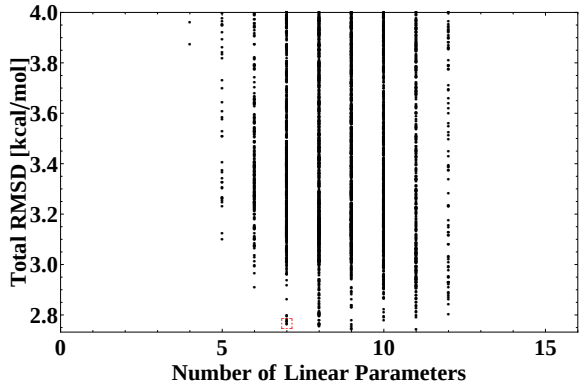

Figure 3: Total RMSDs from 16383 least-squares fits plotted against the number of linear parameters. The boxed point corresponds to the 2y1n1n functional with 7 linear parameters that was picked for self-consistent optimization. The nomenclature is explained in Section 5.

cle 3" heading. While the uniform electron gas (UEG) limit for exchange was enforced from the beginning, the UEG limits for same-spin correlation *and* opposite-spin correlation were allowed to relax and are not satisfied. However, the first-order corrections to same-spin correlation and opposite-spin correlation should be (and are) negative, since the LSDA overestimates the correlation energies of atoms by a factor of 2. On the other hand, the LSDA underestimates the exchange energies of atoms by approximately 10%, and the first-order correction to exchange should be (and is) positive.

It is important to consider the behavior of the ICFs for large gradients in the electron density ($u \approx 1$). The ωB97X-V exchange functional ICF is well-behaved, with a value of 2.630 at $u_{x,\sigma} = 1$. Even though the Lieb-Oxford bound[120] (LOB) was not used as a constraint during the optimization of ωB97X-V, the resulting exchange functional violates the LOB (2.273) by only 0.357. In comparison, the exchange functional ICFs of ωB97X and ωB97X-D have values of 10.189 and 8.396 at $u_{x,\sigma} = 1$, respectively. The ωB97X-V exchange functional exceeds the LOB at $u_{x,\sigma} = 0.874$, which corresponds to $s_{x,\sigma} = 41.707$. According to Perdew and coworkers,[121] only the range corresponding to $0 \leq s_{x,\sigma} \leq 18.562$ is important

for the exchange-correlation energy of atoms. Thus, it is likely that ωB97X-V violates the Lieb-Oxford bound outside of the realm that is considered important for systems of interest. While the same-spin correlation ICF is positive for all values of $u_{c,\sigma\sigma}$, the opposite-spin correlation ICF takes on negative values for $u_{c,\alpha\beta} \geq 0.659$. Although this implies that certain grid points will contribute positive values to the overall correlation energy, Becke witnessed similar behavior for B97 at $u_{c,\alpha\beta} = 0.54$ and concluded that the effects from this feature were of little importance because the sign change occurred far out from the region of chemical relevance.

In order to further investigate the implications of violating the LOB at a value of $u_{x,\sigma} = 0.874$, a molecule from the training set was selected and analyzed. The molecule that was chosen was one of the dianionic sulfate-water cluster isomers with 3 water molecules. With the slightly coarser (75,302) integration grid, this molecule requires 317,100 grid points for the integration of the exchange energy (-60.2615 hartrees). Since there is a value of $u_{x,\sigma}$ that corresponds to each of these grid points, the goal of this analysis was to determine if a significant fraction of these grid points corresponded to values of $u_{x,\sigma} > 0.874$. Figure 4 plots the sum of the grid point exchange energies between $u_{x,\sigma} = 0$ and $u_{x,\sigma} < z$ for $z \in [0, 1]$ in increments of 0.01. The data indicates that the majority of the exchange energy is recovered by $u_{x,\sigma} = 0.3$, and the points that lie between $u_{x,\sigma} = 0.3$ and $u_{x,\sigma} = 1.0$ contribute negligibly. In fact, the grid points between $u_{x,\sigma} = 0$ and $u_{x,\sigma} < 0.874$ contribute 99.9998% of the total exchange energy, while the remaining grid points contribute only an additional -0.076 kcal/mol to the exchange energy. Thus, we believe that it is safe to conclude that the violation of the Lieb-Oxford bound by ωB97X-V has nearly negligible chemical implications. For the 1961 systems in the training and primary test sets, the ratio of the total exchange energy of ωB97X-V (local and nonlocal) to the exchange energy of the LSDA is at least 1.076, at most 1.193, and 1.107 on average.

Figure 5 shows the exchange, same-spin corre-

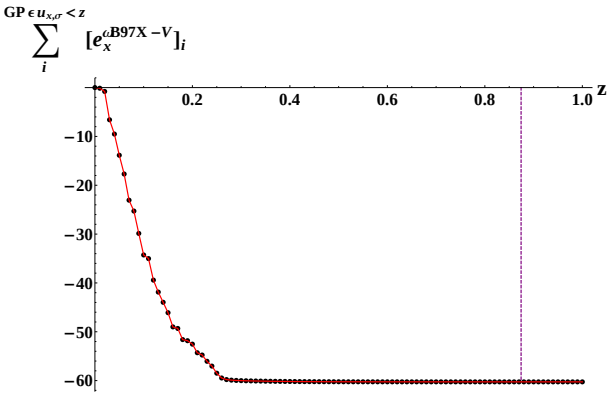

Figure 4: Sum of the exchange energy contributions from all grid points (GP) between 0 and z for a $SO_4{}^{2-}(H_2O)_3$ isomer. The points are evaluated in increments of 0.01. For example, the sixth point from the left corresponds to the sum of the exchange energy contributions from all grid points that fall between $u_{x,\sigma} = 0.0$ and $u_{x,\sigma} = 0.05$. The last point is equivalent to the total exchange energy of the molecule, -60.2615 hartrees. The dashed purple line corresponds to the value of $u_{x,\sigma} = 0.874$ at which the exchange functional of ωB97X-V violates the Lieb-Oxford bound. The grid points between $u_{x,\sigma} = 0$ and $u_{x,\sigma} < 0.874$ contribute 99.9998% of the total exchange energy of the system.

lation, and opposite-spin correlation functional ICF plots for the final ωB97X-V functional, as well as several B97-based functionals, namely, ωB97X, ωB97X-D, and the original B97 functional by Becke. Compared to the ICFs of existing functionals, the exchange functional ICF of ωB97X-V is almost identical to that of B97. While the B97 and ωB97X-V exchange functional ICFs are quadratic, they are quartic for both ωB97X and ωB97X-D. The largest difference among the 4 functionals considered is seen in the same-spin correlation functional ICFs, where ωB97X and ωB97X-D are quartic and oscillatory, B97 is quadratic, and ωB97X-V is linear. In fact, the same-spin correlation functional ICF of ωB97X-V looks liked an averaged-out version of its ωB97X and ωB97X-D counterparts. Finally, the opposite-spin correlation functional ICFs are similar in the region between $u_{c,\alpha\beta} = 0$ and $u_{c,\alpha\beta} = 0.5$, and differ only for large values of $u_{c,\alpha\beta}$.

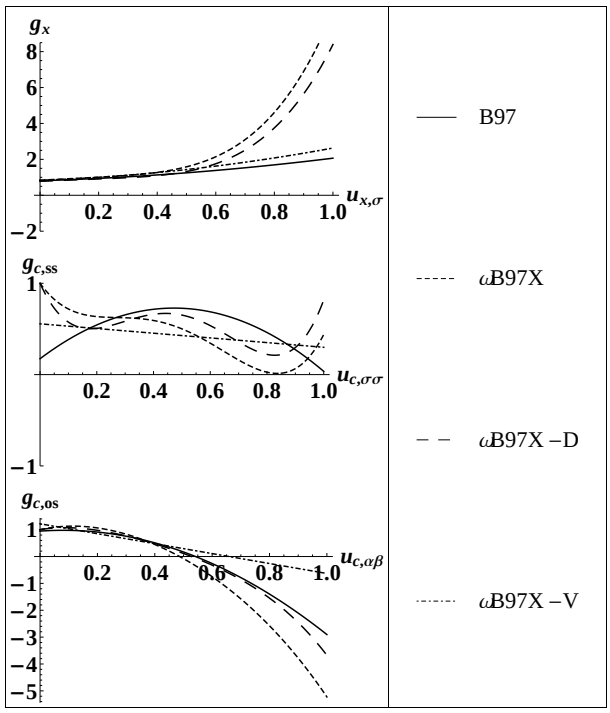

Figure 5: Inhomogeneity correction factors for the exchange, same-spin correlation, and opposite-spin correlation functionals of B97, ωB97X, ωB97X-D, and ωB97X-V.

While DFT is a variational method in principle, non-empirical and semi-empirical exchange-correlation functionals that attempt to approximate the exact exchange-correlation functional are not guaranteed to provide variational energies. In order to assess the variational validity of ωB97X-V, the absolute energies of the 6 systems from Reference 122 (along with the absolute energy of the argon atom from Reference 87) were computed and compared to the best available variational values. Table 5 contains the difference (in kcal/mol) between the DFT energy and the best available variational energy, with negative entries corresponding to non-variational energies and positive entries corresponding to variational energies. The UGBS basis set[123] was used with the (500,974) grid for local xc functionals and the (99,590) grid for the VV10 NLC functional. The only functionals that provide variational energies for all 7 test systems are PBE and LC-VV10. ωB97X-V provides a non-variational absolute energy for the lithium atom, but it is lower by only -0.68 kcal/mol. The rest of the functionals have at least 4 non-variational entries. It is surprising that while LC-VV10 has variational energies for all 7 cases, its local version, VV10, has non-variational energies for all 7 cases.

7 Results and Discussion

7.1 Performance

Thus far, we have completed the training and selection of the ωB97X-V functional in a manner that is internally consistent, such that the resulting functional emerges as the fittest of over 16000 candidate functionals. The next step is to compare against a selection of existing density functionals across the training set, primary test set, and the hitherto unused secondary test set. The density functionals that were benchmarked along with ωB97X-V were selected for reasons that will be briefly described in this section.

PBE is arguably the best unparameterized density functional available, while B3LYP is certainly the most popular density functional to date. B97 is the forefather of dozens of parameterized density functionals (including ωB97X-

Table 5: Difference (in kcal/mol) between the DFT energy and the best available variational energy for 5 atoms and 2 anions. Entries that are negative correspond to non-variational values. The UGBS basis set was used with the (500,974) grid for local xc functionals and the (99,590) grid for the VV10 NLC functional.

System	PBE	B3LYP	B97	B97-D	VV10	LC-VV10	ωB97X-D	ωB97X-V	M06-L	M06	M06-2X	M11-L	M11
H-	2.11	-4.40	0.50	-5.36	-1.67	4.11	-2.69	1.05	1.13	2.49	4.07	-21.14	-3.03
He	6.77	-7.22	-3.94	-8.09	-8.01	4.13	-3.73	0.12	-7.46	-5.02	-1.02	-10.66	-3.46
Li	9.97	-9.35	-6.45	-6.20	-15.63	12.24	-8.29	-0.68	-8.05	-6.98	-3.92	-36.67	-6.70
Li-	13.26	-7.10	-3.19	-6.84	-11.51	17.43	-5.68	3.91	-7.42	-4.22	-0.13	-31.37	-6.01
Be	23.47	-3.75	0.14	1.47	-15.21	28.57	0.10	2.73	0.51	2.09	-0.07	-38.91	-2.29
Ne	44.67	-27.21	-2.67	1.79	-110.44	42.42	-11.13	0.58	-16.04	-11.50	-4.01	-17.51	-27.43
Ar	121.70	-17.44	34.72	-38.17	-211.12	129.85	-8.19	40.53	-6.11	2.23	-1.07	-40.45	-7.70

V). Since the 3 functionals mentioned thus far are ill-equipped for describing weak dispersive interactions, dispersion-corrected variants are commonly employed as well. While the dispersion tails of PBE-D2, B3LYP-D2, and B97-D2 were optimized onto the existing parent functional, Grimme's B97-D functional was the first attempt at simultaneously parameterizing the linear parameters of a density functional with a dispersion tail. Since the VV10 nonlocal correlation functional is a vital component of ωB97X-V, the 2 existing density functionals that incorporate the VV10 NLC functional (VV10 and LC-VV10) must be benchmarked. With respect to dispersion-corrected RSH GGA density functionals, the direct predecessor to ωB97X-V is ωB97X-D, and it is important to confirm that ωB97X-V improves upon its older counterpart. Finally, from the 10 Minnesota functionals mentioned in Section 1, M06-L, M06, M06-2X, M11-L and M11 were chosen.

Table 6 contains the RMSDs for all of the datasets in the training, primary test, and secondary test sets for ωB97X-V and 15 existing density functionals (PBE, PBE-D2, B3LYP, B3LYP-D2, B97, B97-D2, B97-D, VV10, LC-VV10, ωB97X-D, M06-L, M06, M06-2X, M11-L, and M11). Table 7 contains information regarding the benchmarked functionals.

Of the 16 benchmarked density functionals, M06-2X has the best overall performance for thermochemistry (3.21 kcal/mol) and ωB97X-V has the best overall performance for noncovalent interactions (0.32 kcal/mol). After M06-2X, the next best density functionals for thermochemistry are ωB97X-V and ωB97X-D, with RMSDs of 3.61 kcal/mol. After ωB97X-V, the next best density functionals for noncovalent interactions are M06-L and B97-D2, with RMSDs of 0.47 and 0.48 kcal/mol, respectively. Before the individual datasets are discussed, the overall performance of the functionals for thermochemistry (TC) and noncovalent interactions (NC) will be discussed.

Overall, the performance of ωB97X-V is identical to that of ωB97X-D for thermochemistry, but more than 0.20 kcal/mol better for noncovalent interactions. As a sanity check, it is important to verify that ωB97X-V drastically improves upon VV10. ωB97X-V reduces the overall thermochemistry RMSD of its counterpart by a factor of 2.7. Furthermore, it improves upon the overall NC RMSD of VV10 by a factor of 4.3. In addition to outperforming VV10, ωB97X-V should perform much better than LC-VV10 as well, since its local GGA components have been carefully parameterized. As expected, ωB97X-V reduces the overall TC and NC RMSDs of LC-VV10 by factors of 2. The functional forms of ωB97X-V and M11 are similar, since both functionals are range-separated hybrids that have exchange-correlation functionals that depend on the density as well as its gradient. However, the exchange-correlation functional of M11 additionally depends on the kinetic energy density, while ωB97X-V includes the VV10 NLC functional instead. Furthermore, M11 has 4 times more parameters than ωB97X-V. Thus, it is quite surprising that ωB97X-V outperforms M11 with respect to both overall thermochemistry and overall noncovalent interactions. While M11-L is the newest local meta-

GGA Minnesota functional, its older counterpart, M06-L, outperforms it with respect to both overall thermochemistry and overall noncovalent interactions. M06-2X is better than M06 by a factor of 1.3 for thermochemistry, while the reverse is true for noncovalent interactions. It is interesting to compare the performance of the functionals with the DFT-D2 dispersion tails to their parent functionals to assess the extent to which the addition of the tail enhances the performance of the parent functional for noncovalent interactions. Furthermore, it is desirable that the parent functional's performance for thermochemistry remains unaltered. The addition of DFT-D2 to B3LYP improves its overall NC RMSD by a factor of 3, and also slightly improves its performance for thermochemistry. With Becke's B97 functional, the improvement for noncovalent interactions is even more dramatic, as the DFT-D2 tail cuts the overall NC RMSD of B97 by more than a factor of 5. For PBE, however, the addition of the DFT-D2 tail enhances the description of noncovalent interactions very slightly, and worsens the TC RMSD.

Since it would be tedious to individually address the performance of the benchmarked density functionals on the 47 datasets in Table 6, only a handful of datasets will be discussed. The TAE_nonMR124 dataset is comprised of the atomization energies of small molecules computed with the Weizmann-4 (W4) theory. ωB97X-V has an RMSD of 3.34 kcal/mol on this dataset of 124 datapoints, and is second only to M06-2X (3.25 kcal/mol). Furthermore, the performance of ωB97X-V is more than 0.30 kcal/mol better than that of ωB97X-D, and more than 1 kcal/mol better than that of M11. The DBH24 dataset contains 24 forward and reverse barrier heights computed (at least) with the Weizmann-3.2 (W3.2) theory. M06-2X performs the best for this dataset (1.12 kcal/mol), followed by M11 (1.48 kcal/mol) and ωB97X-V (1.81 kcal/mol). The AlkAtom19 dataset contains the atomization energies of 19 alkanes ranging from methane to octane. Since these molecules are much larger than the ones found in TAE_nonMR124, it is important to assess the performance of ωB97X-V on this dataset to determine if the satisfactory performance for the atomization energies of smaller molecules is transferable to larger molecules. The RMSD of ωB97X-V on AlkAtom19 (0.71 kcal/mol) is 7 times smaller than that of M06-2X (5.27 kcal/mol) and 5 times smaller than that of M11 (3.94 kcal/mol). ωB97X-V beats ωB97X-D by a factor of 4 on the AlkAtom19 dataset, and is outperformed only by B3LYP-D2 (0.64 kcal/mol). However, it is clear that the surprisingly small RMSD of B3LYP-D2 is a fortuitous result, since the dispersion tail contributes only to the absolute energies of the alkanes (and not the atoms). Thus, while B3LYP drastically underestimates the atomization energies of the alkanes in AlkAtom19, the dispersion tail manages to lower the absolute energies of the alkanes to overcome this underestimation. If one considers PBE (which drastically overestimates the atomization energies on its own), the addition of the same dispersion tail makes things much worse.

In recent years, Hobza's S22 and S66 datasets have been quite popular for benchmarking the performance of density functionals on noncovalent interactions. The RMSD of ωB97X-V on the S22 dataset is 0.23 kcal/mol, which is almost 2 times smaller than the next best functional, ωB97X-D (0.41 kcal/mol). It is important to emphasize that the parameters of ωB97X-D were trained on the S22 dataset, while the parameters of ωB97X-V were validated, but not trained, on the S22 dataset. From the Minnesota functionals, M06-L has the best performance for S22, with an RMSD of 0.43 kcal/mol, followed by M06-2X (0.47 kcal/mol) and M11 (0.58 kcal/mol). On the S66 dataset, ωB97X-V has the lowest RMSD at 0.18 kcal/mol, with the next best functional (M06-2X) having an RMSD of 0.29 kcal/mol. The most recent dataset by Hobza is A24, which consists of very accurate CCSD(T)/CBS binding energies for small molecules. ωB97X-V performs the best for this dataset as well, with an RMSD of only 0.09 kcal/mol. The 5 Minnesota functionals have RMSDs larger than 0.20 kcal/mol, and the only functionals that comes close to ωB97X-V are ωB97X-D and LC-VV10, with RMSDs of 0.15 kcal/mol.

The last dataset from Hobza that will be discussed is X40, which is comprised of binding energies of halogenated molecules. ωB97X-V has the best performance for this dataset, with an RMSD of 0.21 kcal/mol. M06-2X performs satisfactorily on X40 as well, with an RMSD of 0.28 kcal/mol, while its family members, M06-L (0.48 kcal/mol), M06 (0.57 kcal/mol), M11-L (1.23 kcal/mol), and M11 (0.54 kcal/mol), have RMSDs that are at least twice as large as that of ωB97X-V.

Herbert and coworkers recently reported[91] that density functionals such as LC-VV10 and M06-2X perform poorly for halide-water clusters. Specifically, the systems of interest are $F^-(H_2O)_n$ and $Cl^-(H_2O)_n$, for $n = 1 - 6$. Using the same geometries and reference values, the RMSDs for these 2 datasets were computed for the 16 density functionals in Table 6. ωB97X-V has the best performance for the interactions containing the fluoride anion, with an RMSD of 0.36 kcal/mol. In comparison, the Minnesota functionals perform at least 2.5 times worse. The performance of ωB97X-D is 4 times worse than the performance of its new counterpart, and the only density functional that comes close to ωB97X-V is B97-D2, with an RMSD of 0.59 kcal/mol. However, for the interactions that contain the chloride anion, B97-D2 has the best performance, with an RMSD of only 0.33 kcal/mol. Surprisingly, PBE comes in at second with an RMSD of 0.59 kcal/mol, while ωB97X-V has the third best RMSD at 0.67 kcal/mol. While the Minnesota functionals tend to perform slightly better on this dataset than on HW6F, their RMSDs are still at least 4.5 times larger than that of B97-D2. Both the H2O6Rel and CYCONF datasets in the secondary test set are meant to gauge the performance of density functionals for the relative energies of conformers. ωB97X-V has the best performance for both datasets, with RMSDs of 0.07 kcal/mol and 0.11 kcal/mol, respectively. For H2O6Rel, the next best density functional is ωB97X-D with an RMSD of 0.18 kcal/mol, while the Minnesota functionals have RMSDs larger than 1 kcal/mol. In addition, the RMSD of ωB97X-V (0.11 kcal/mol) for CYCONF is 3 times smaller than that of ωB97X-D (0.41 kcal/mol), but comparable to that of M06 (0.16 kcal/mol). The last dataset in the secondary training set is DS14, which contains binding energies for systems that contain divalent sulfur. Since the molecules in this dataset are small, the reference values were computed at the CCSD(T)/CBS level (with counterpoise corrections), with the following contributions: HF/aQZ + MP2/a(TQ)Z + (CCSD(T)-MP2)/aTZ. The performance of ωB97X-V on DS14 is near perfect, with an RMSD of only 0.05 kcal/mol. The next best density functional, ωB97X-D, has an RMSD that is 3 times larger (0.18 kcal/mol). M06-2X has the best performance on DS14 from the Minnesota functionals, but its RMSD of 0.20 kcal/mol is still 4 times larger than that of ωB97X-V.

In Figure 6, the potential energy curves (PEC) for the helium dimer (He_2) and argon dimer (Ar_2) are shown. The argon dimer is an important case to consider for ωB97X-V, since the datapoints corresponding to 3 rare-gas dimers (Ne_2, Ar_2, and NeAr) were weighted by 25000 in the calculation of the primary test set RMSD. While the parameters of ωB97X-V were not explicitly optimized on the argon dimer PEC, the functional form that was ultimately selected (2y1n1n) was influenced by its good performance for these 3 dimers. Thus, it is not surprising that the ωB97X-V PEC for the argon dimer in Figure 6 is basically superimposed on the "Reference" PEC (Tang-Toennies). Furthermore, it is satisfactory that the good performance of VV10 has been maintained. Besides confirming that the functional selection strategy worked exactly as intended, Figure 6 highlights a disadvantage of functionals that were trained without checking for transferability in the selected linear parameters. ωB97X-D predicts an equilibrium bond distance that is 0.5 Å too long and underbinds the dimer. LC-VV10, M06-L, and M06-2X perform comparably to ωB97X-D, while the biggest surprises are the results produced by the 2 newest Minnesota functionals, M11-L and M11. M11-L has an artificial inflection point at the correct equilibrium distance, but binds the dimer at more than 5 Å. On the other hand, M11 binds the dimer

Table 6: RMSDs in kcal/mol for all of the datasets in the training, primary test, and secondary test sets for ωB97X-V and 15 existing density functionals. The datasets above the first thick black line are in the training set, the datasets between the first and second thick black lines are in the primary test set, while the datasets below the second thick black line are in the secondary test set. Within the training, primary test, and secondary test sets, datasets above the thin black line contain thermochemistry (TC) datapoints, while datasets below the thin black line contain noncovalent interactions (NC) datapoints. The last section of the table contains overall unweighted statistics. For comparison to B3LYP-D2, the All TC RMSD of B3LYP-D3 is 4.7 kcal/mol, while the All NC RMSD is 0.8 kcal/mol.

Dataset	PBE	PBE-D2	B3LYP	B3LYP-D2	B97	B97-D2	B97-D	VV10	LC-VV10	ωB97X-D	ωB97X-V	M06-L	M06	M06-2X	M11-L	M11
HAT707	7.81	7.79	4.31	4.28	3.98	3.98	5.62	7.23	6.81	4.14	4.28	5.86	4.83	3.63	5.43	4.28
BDE99	8.89	8.98	4.07	3.88	3.23	3.18	4.58	6.63	5.39	3.03	3.38	6.14	3.72	2.99	4.61	4.10
TAE_nonMR124	16.72	16.94	5.43	5.28	4.39	4.06	5.18	12.46	5.30	3.65	3.34	5.54	3.94	3.24	6.62	4.37
SN13	5.74	5.36	2.33	1.74	1.28	0.97	4.20	3.67	2.65	0.96	1.01	1.58	2.03	1.01	3.19	2.19
ISOMER20	4.54	4.53	2.35	2.29	2.34	2.30	3.83	4.34	1.85	1.86	1.64	4.11	2.53	1.47	4.46	1.94
DBH24	10.05	10.37	4.83	5.28	4.05	4.36	7.18	9.86	3.02	2.07	1.81	5.38	2.97	1.12	3.54	1.48
EA6	4.71	4.71	3.49	3.49	1.45	1.45	2.07	5.28	2.10	1.89	2.34	2.39	1.91	1.95	6.17	1.33
IP6	5.07	5.07	6.16	6.16	3.19	3.19	2.68	7.64	5.03	3.01	3.76	2.26	3.23	2.86	3.36	5.79
AE8	30.54	30.54	15.89	15.89	2.25	2.25	6.94	64.43	29.82	4.67	1.77	9.22	5.52	1.28	15.27	9.23
SW49Rel345	0.90	1.55	0.39	1.17	0.30	0.79	1.22	1.26	0.36	1.01	0.33	0.53	0.60	0.35	0.22	0.17
SW49Bind345	1.22	2.59	3.07	1.72	3.44	0.69	1.35	2.47	0.58	0.98	0.29	0.60	0.72	0.95	1.54	0.25
NBC10A2	0.91	0.28	1.51	0.20	1.19	0.08	0.08	0.05	0.12	0.13	0.09	0.15	0.28	0.11	0.54	0.16
HBC6A	0.54	1.45	1.27	0.94	1.37	0.39	0.77	1.13	1.25	0.61	0.39	0.36	0.31	0.59	0.68	0.46
BzDC215	1.07	0.69	1.94	0.57	1.54	0.36	0.39	0.22	0.60	0.41	0.27	0.17	0.25	0.60	0.34	0.65
EA7	2.27	2.28	3.52	3.54	2.54	2.55	3.86	3.57	4.19	2.45	2.28	6.07	2.94	1.97	6.44	1.08
IP7	4.28	4.28	5.22	5.22	3.41	3.41	4.03	4.76	5.30	3.26	2.97	3.11	2.93	3.24	2.89	4.56
Gill12	8.24	6.56	5.71	3.27	5.69	3.84	4.84	6.08	2.58	3.24	2.32	6.71	3.82	1.78	5.60	2.58
AlkAtom19	15.83	26.21	14.63	0.64	19.78	9.28	10.48	5.85	19.04	2.90	0.71	8.11	4.63	5.27	29.35	3.94
AlkIsomer11	2.87	0.40	3.96	0.59	3.78	0.57	0.33	0.84	0.13	1.04	0.67	0.95	0.22	0.15	0.74	0.56
AlkIsod14	4.88	0.42	6.57	0.35	6.44	1.93	0.57	2.01	1.09	2.31	1.80	3.86	1.68	1.65	2.06	2.11
HTBH38	9.97	10.57	4.81	5.49	4.53	5.12	7.63	9.22	1.50	2.57	2.28	4.62	2.21	1.26	1.86	1.68
NHTBH38	10.20	10.53	5.41	5.84	3.83	4.15	7.12	10.79	3.38	1.73	1.64	4.79	2.64	1.69	3.72	1.49
SW49Rel6	1.20	2.16	0.29	1.59	0.16	1.01	1.65	1.72	0.52	1.34	0.37	0.80	0.89	0.42	0.21	0.28
SW49Bind6	2.40	4.51	6.31	2.92	7.18	0.90	2.50	4.56	0.91	0.99	0.36	0.57	0.92	1.61	3.38	0.67
NNTT41	0.02	0.09	0.08	0.05	0.03	0.06	0.07	0.03	0.02	0.15	0.02	0.04	0.12	0.05	0.32	0.02
AATT41	0.13	0.05	0.30	0.08	0.19	0.05	0.16	0.02	0.07	0.21	0.02	0.15	0.23	0.08	0.46	0.17
NATT41	0.02	0.09	0.14	0.02	0.06	0.05	0.08	0.04	0.03	0.15	0.02	0.05	0.13	0.03	0.35	0.04
NBC10A1	3.29	0.19	4.77	0.26	3.98	0.67	0.20	0.27	0.15	0.41	0.23	0.26	0.58	0.43	0.47	0.69
NBC10A3	2.57	0.28	3.77	0.29	3.20	0.54	0.19	0.17	0.06	0.27	0.37	0.47	0.69	0.63	0.83	0.80
WATER27	3.46	7.58	3.63	4.63	4.72	1.42	2.56	7.07	3.35	1.48	1.42	1.34	1.70	3.66	4.60	1.62
HW30C4	0.52	0.71	1.12	0.53	0.83	0.35	0.40	0.43	0.30	0.35	0.20	0.35	0.33	0.46	0.48	0.38
NCCE31	1.97	2.45	1.00	1.05	0.93	0.84	1.27	2.67	0.53	0.38	0.27	1.23	0.56	0.36	0.75	0.51
S22x5	2.91	0.65	3.99	0.61	3.64	0.71	0.40	0.59	0.48	0.43	0.41	0.42	0.80	0.47	0.94	0.55
S66x8	2.19	0.64	3.17	0.65	2.73	0.35	0.43	0.50	0.34	0.44	0.22	0.31	0.48	0.35	0.83	0.42
S22	3.50	0.70	4.74	0.74	4.25	0.60	0.54	0.63	0.51	0.41	0.23	0.43	0.77	0.47	0.91	0.58
S66	2.59	0.63	3.71	0.62	3.16	0.36	0.52	0.52	0.31	0.52	0.18	0.36	0.53	0.29	0.81	0.41
G21EA	3.97	3.96	3.54	3.54	1.83	1.84	3.00	4.60	3.89	1.98	2.27	4.54	2.46	1.99	6.56	2.40
G21IP	4.81	4.81	4.86	4.86	3.48	3.48	4.47	5.43	5.23	3.82	3.57	5.60	3.78	3.49	4.50	4.64
PA8	1.64	1.71	1.20	1.49	2.41	2.67	3.70	1.77	2.74	2.95	2.20	3.36	2.21	1.98	3.57	1.35
A24	0.46	0.59	1.05	0.39	0.75	0.26	0.32	0.41	0.15	0.15	0.09	0.23	0.25	0.28	0.46	0.27
X40	1.63	0.74	2.48	0.47	2.08	0.43	0.59	0.63	0.41	0.49	0.21	0.48	0.57	0.28	1.23	0.54
H2O6Rel	1.77	0.35	2.31	0.59	2.26	0.20	0.41	0.38	0.22	0.18	0.07	1.75	2.10	1.76	1.01	1.45
H2O6Bind	0.90	5.74	3.76	4.10	5.27	0.33	3.82	5.70	2.68	1.55	0.70	0.97	1.01	2.25	4.00	0.67
HW6F	1.72	3.64	4.64	2.78	5.83	0.59	4.34	3.71	2.55	1.46	0.36	2.47	2.11	4.91	1.04	2.95
HW6Cl	0.59	4.74	5.27	2.05	5.49	0.33	3.25	5.26	2.84	0.78	0.67	1.61	2.10	3.65	2.73	2.25
CYCONF	0.95	0.98	0.53	0.32	0.49	0.37	0.56	0.57	0.78	0.41	0.11	0.39	0.16	0.30	0.57	0.51
DS14	1.10	0.57	1.94	0.28	1.55	0.25	0.37	0.52	0.12	0.18	0.05	0.25	0.34	0.20	0.59	0.30
All TC	9.90	10.35	5.11	4.59	4.74	3.97	5.56	9.81	6.79	3.61	3.60	5.63	4.18	3.21	6.68	3.97
All NC	2.00	1.49	2.96	1.01	2.71	0.48	0.82	1.38	0.73	0.54	0.32	0.47	0.60	0.78	1.07	0.56
Training TC	10.27	10.33	4.71	4.66	3.89	3.83	5.43	10.44	6.86	3.82	3.88	5.75	4.45	3.36	5.64	4.23
Training NC	0.89	1.33	1.74	0.91	1.66	0.44	0.76	1.09	0.86	0.61	0.32	0.34	0.38	0.59	0.68	0.48
Primary Test TC	9.76	12.33	7.17	4.43	8.28	5.00	6.79	7.87	7.32	2.42	1.89	5.25	2.86	2.45	11.05	2.32
Primary Test NC	2.29	1.45	3.28	0.99	2.96	0.50	0.68	1.35	0.61	0.50	0.32	0.42	0.59	0.68	1.11	0.51
Secondary Test TC	4.25	4.26	4.12	4.14	2.86	2.89	3.91	4.84	4.54	3.17	3.01	5.01	3.20	2.87	5.26	3.68
Secondary Test NC	1.27	2.12	2.59	1.39	2.74	0.36	1.65	2.15	1.17	0.65	0.29	0.92	0.99	1.60	1.50	1.02

Table 7: Details for the density functionals from Table 6. GH stands for global hybrid, RSH stands for range-separated hybrid, DC stands for dispersion correction, and NLC stands for nonlocal correlation. The column labeled "#" lists the number of parameters that were optimized on a training set for the specific functional. c_x refers to the percentage of exact exchange.

Property	#	c_x	Year	Class	Rung	Ref.
PBE	0	0	1996	GGA	2	124
PBE-D2	1	0	2006	GGA w/ DC	2	48
B3LYP	3	20	1993	GH GGA	4	125
B3LYP-D2	4	20	2006	GH GGA w/ DC	4	48
B97	10	19	1997	GH GGA	4	4
B97-D2	11	19	2011	GH GGA w/ DC	4	79
B97-D	10	0	2006	GGA w/ DC	2	48
VV10	2	0	2010	GGA w/ NLC	2	62
LC-VV10	3	0-100	2010	RSH GGA w/ NLC	4	62
ωB97X-D	15	22.2-100	2008	RSH GGA w/ DC	4	43
ωB97X-V	10	16.7-100	2013	RSH GGA w/ NLC	4	
M06-L	34	0	2006	meta-GGA	3	19
M06	33	27	2008	GH meta-GGA	4	23
M06-2X	30	54	2008	GH meta-GGA	4	23
M11-L	43	0	2012	meta-GGA	3	20
M11	40	42.8-100	2011	RSH meta-GGA	4	26

very weakly, with an equilibrium bond length that is too long. Since a (500,974) grid was used for computing the local xc functionals, it is unlikely that the strange behavior of the M11-L functional is related to the integration of the xc functional. Since the argon dimer PEC technically influenced the functional form of ωB97X-V, the PEC for the helium dimer is shown on the left in Figure 6 as a completely independent test case. The performance of ωB97X-V is superb for this dimer as well. Neither B3LYP nor B3LYP-D2 bind the helium dimer, while M11 binds the dimer with an equilibrium bond length that is too long. PBE, PBE-D2, M06, and M06-2X all overbind the dimer, but predict reasonable equilibrium bond lengths.

7.2 Coronene Dimer

The largest intermolecular interactions in the training set for ωB97X-V are the 12 $SO_4{}^{2-}(H_2O)_5$ isomers from the SW49Rel345 and SW49Bind345 datasets. In the aTZ basis set, these molecules have 694 basis functions. In the primary test set, the largest intermolecular interactions are the 5 adenine-thymine complexes from the S22x5 dataset with 1127 basis functions in the aTZ basis set. In order to assure that ωB97X-V can be successfully applied to even larger interactions, the binding energy of the parallel-displaced coronene dimer was computed in the aDZ and aTZ basis sets (1320 and 2760 basis functions for the dimer, respectively). The binding energy in the aDZ basis set was counterpoise-corrected (CP), while counterpoise corrections were not used (noCP) in the aTZ basis set. The resulting binding energies for the functionals from Table 6 are shown in Table 8.

While there is no definitive reference value for the binding energy of the parallel-displaced coronene dimer, 2 recent attempts[126,127] at determining a "CBS" value resulted in binding energies of -20.0 kcal/mol and -24.4 kcal/mol. Furthermore, 2 methods that have been shown to have good performance for dispersion-bound systems (attenuated (aTZ) MP2[128] and MP2.5[129]) give values of -21.3 kcal/mol and -22.8 kcal/mol, respectively. Thus, it is safe to assume that the binding energy of the parallel-displaced coronene dimer is between -20.0 and -25.0 kcal/mol.

The noCP aTZ ωB97X-V binding energy of -22.4 kcal/mol is right in the middle of this range, while the 5 Minnesota functionals underbind the dimer. As expected, the GGA functionals without dispersion corrections fail to bind the dimer (PBE, B3LYP, B97), and even though the DFT-D2 dispersion tail adds -22.4, -31.3, and -22.4 kcal/mol to the binding energy of the parent functionals, respectively, PBE-D2 and B97-D2 still underbind the dimer. However, due to the large s_6 parameter of B3LYP-D2, its noCP aTZ binding energy falls within the aforementioned range. The binding energies of B97-D, VV10, LC-VV10, and ωB97X-D are quite close to that of ωB97X-V, and lie between -20.0 and -25.0 kcal/mol for both the CP aDZ and noCP aTZ calculations. The last column of Table 8 lists the difference (kcal/mol) between the CP aDZ and noCP aTZ binding energies for the 16 functionals. It is certainly desirable for this difference to be as small as possible, since the noCP aTZ calculation is at least 10 times more costly than the CP aDZ calculation. For LC-VV10, ωB97X-D, ωB97X-

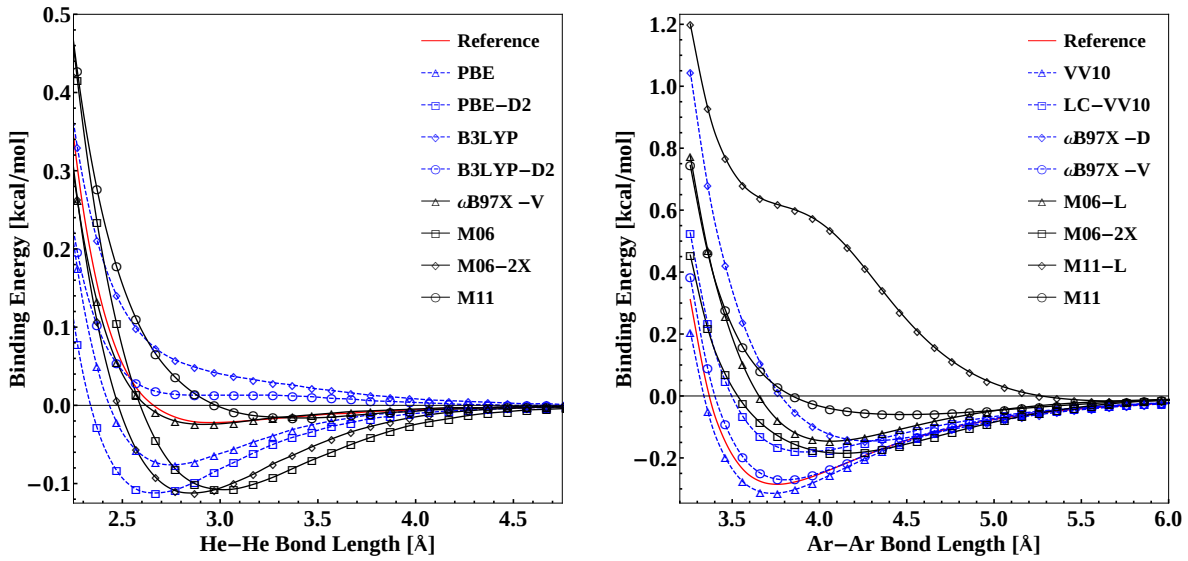

Figure 6: Potential energy curves for the helium dimer and the argon dimer. A (500,974) grid was used for computing local xc functionals and a (99,590) grid was used for computing the contribution from the VV10 NLC functional. The calculations were performed with the aug-cc-pVQZ basis set without counterpoise corrections.

V, and M06-L, this difference is less than 0.60 kcal/mol, while for M11-L and M11, the difference is larger than 2 kcal/mol.

7.3 Geometries

To assess the ability of ωB97X-V to calculate accurate geometries, 4 sets of geometries were benchmarked. The first set, A21, includes the 21 equilibrium geometries from the A24 dataset, which were originally optimized (with counterpoise corrections) at a very high level of theory (HF/aQZ + MP2/a(TQ)Z + (CCSD(T)-MP2)/aDZ) with the intention of serving as a benchmark. The DFT benchmark optimizations were performed in the aTZ basis set with a (99,590) grid for local xc functionals and the SG-1 grid for the VV10 NLC functional. The RMSD between each initial (A21) geometry and final (optimized) geometry was calculated with the Kabsch algorithm.[130] Each row in the second column of Table 9 contains the RMSD of the 21 RMSDs generated by the Kabsch algorithm. The RMSD of ωB97X-V for these 21 interactions is an outstanding 0.58 pm. The RMSD of the next best functional, B97-D2, is 3 times larger than that of ωB97X-V. Furthermore, the ωB97X-V result is more than 5 times better than that of ωB97X-D, and more than 7 times better than that of the Minnesota functionals. The next dataset includes the equilibrium bond lengths of 6 rare-gas dimers: He_2, HeNe, HeAr, Ne_2, NeAr, and Ar_2. The reference values were taken from the Tang-Toennies potential model,[116] and the optimizations were performed in the aTZ basis set with a (500,974) grid for local xc functionals and a (75,302) grid for the VV10 NLC functional. ωB97X-V has the best performance, with an RMSD of 7.91 pm, while VV10 follows closely behind at 8.07 pm. From the Minnesota functionals, M06-2X and M06-L perform well, while M11-L has an RMSD of almost 1 Å. From the dispersion-corrected functionals, B97-D2, B97-D, and PBE-D2 perform decently, while ωB97X-D and B3LYP-D2 perform poorly. The third set of geometries, taken from the work of Tentscher and Arey,[131] contains 18 bond lengths of 18 small radicals. For this set of geometries, M06-L performs the best, followed by B97-D2 and B3LYP-D2. In general, the bond length RMSDs are very small, ranging from 0.69 pm to 2.32 pm. ωB97X-V performs decently, with an RMSD of 1.15 pm. The

Table 8: Binding energies in kcal/mol for the parallel-displaced coronene dimer for the density functionals from Table 6. noCP means non-counterpoise-corrected while CP means counterpoise-corrected. In the aDZ basis set, the dimer has 1320 basis functions, while it has 2760 basis functions in the aTZ basis set. The column labeled "Δ" contains the difference between the CP aDZ and noCP aTZ binding energies for each functional.

Functional	CP aDZ	noCP aTZ	Δ
PBE	5.26	4.63	-0.64
PBE-D2	-17.12	-17.76	-0.64
B3LYP	11.90	10.52	-1.38
B3LYP-D2	-19.43	-20.81	-1.38
B97	8.22	7.33	-0.89
B97-D2	-14.17	-15.06	-0.89
B97-D	-21.42	-22.36	-0.94
VV10	-20.95	-22.07	-1.12
LC-VV10	-23.75	-23.27	0.48
ωB97X-D	-24.36	-24.36	-0.01
ωB97X-V	-21.97	-22.40	-0.43
M06-L	-17.10	-17.68	-0.58
M06	-14.72	-14.62	0.11
M06-2X	-18.22	-17.47	0.75
M11-L	-14.49	-17.64	-3.15
M11	-17.81	-15.71	2.09

last set of geometries, taken from Bak et al.,[132] contains 28 bond lengths of 19 small molecules. The reference geometries were computed at the CCSD(T)/cc-pCVQZ level of theory and validated against experimental results. For this set of geometries, M06-L, B3LYP-D2, and B97-D2 perform very well, followed by B97-D and ωB97X-V. For the last 2 datasets, the optimizations were carried out in the aTZ basis set with a (75,302) grid for local xc functionals and SG-1 for the VV10 NLC functional.

Table 9: RMSDs from the 4 geometry datasets discussed in Section 7.3. For the latter 3 datasets, the entries are bond length RMSDs. For the A21 dataset, an RMSD was calculated for each molecule using the Kabsch algorithm. Each row in the second column contains the RMSD of the 21 RMSDs generated by the Kabsch algorithm.

RMSD [pm]	A21	Rare-gas	Arey	Bak
PBE-D2	8.33	20.94	1.30	1.20
B3LYP-D2	5.95	84.48	0.82	0.61
B97-D2	1.78	15.19	0.81	0.66
B97-D	5.38	18.55	1.10	0.92
VV10	7.38	8.07	1.43	1.39
LC-VV10	2.93	13.05	1.82	1.74
ωB97X-D	3.34	36.34	1.28	1.11
ωB97X-V	0.58	7.91	1.15	0.98
M06-L	7.02	14.06	0.69	0.60
M06	4.22	34.03	1.46	1.27
M06-2X	4.90	12.65	1.67	1.38
M11-L	4.69	96.02	2.32	2.31
M11	5.00	21.10	1.68	1.36

8 Using ωB97X-V

Even though ωB97X-V was trained without counterpoise corrections in the aTZ basis set for noncovalent interactions and without counterpoise corrections in the aQZ basis set for thermochemistry, it is inevitable that the functional will be used with different basis sets. As a result, this section explains how the functional should be used and what basis sets are recommended. Ideally, calculations with ωB97X-V should be run as close as possible to the basis

set limit. As an example, the binding energy of the water dimer (NCCE31 dataset geometry) was computed with and without counterpoise corrections with the aug-cc-pVXZ (X = D, T, Q, 5) [aXZ] family of basis sets. The resulting counterpoise-corrected binding energies (CP) in kcal/mol are $\{-4.96, -4.98, -5.01, -5.00\}$, while the resulting non-counterpoise-corrected binding energies (noCP) in kcal/mol are $\{-5.18, -5.03, -5.04, -5.01\}$. Since ωB97X-V was trained without counterpoise corrections in the aTZ basis set for noncovalent interactions, the corresponding value of -5.03 kcal/mol is the "best" value. However, the noCP aQZ and noCP a5Z binding energies differ from the noCP aTZ binding energy by 0.02 kcal/mol at most. Thus, using basis sets that are larger and contain higher angular momentum functions than the ones used for training will not degrade the performance of the functional. Regarding the aDZ basis set, it is clear that this basis set should not be used with ωB97X-V without counterpoise corrections, since the basis set superposition error (BSSE) at the aDZ basis set level is larger than 0.20 kcal/mol for the water dimer. However, since the difference between the noCP aTZ and CP aDZ binding energies for the water dimer is only 0.06 kcal/mol, the aDZ basis set can be used with counterpoise corrections if necessary. Furthermore, Table 8 indicates that the difference between the noCP aTZ and CP aDZ binding energies for the parallel-displaced coronene dimer is less than 0.50 kcal/mol. Thus, if a noCP aTZ calculation is impractical, a CP aDZ calculation will suffice.

Similar tests were performed on 3 dimers from the NCCE31 dataset (water, hydrogen fluoride, and ammonia) with a variety of basis sets from the EMSL basis set exchange,[133,134] and the results are summarized in Table 10. If the MG3S[135] or LP[136,137] basis sets are desired, we highly recommend that counterpoise corrections be utilized, since ωB97X-V produced poor results when these basis sets were employed without counterpoise corrections. For example, the binding energy for the water dimer in the MG3S basis set is -4.99 kcal/mol with counterpoise corrections and -5.28 kcal/mol without. Compared to the CCSD(T)/CBS estimate of approximately -5.00 kcal/mol, it is clear that the CP MG3S value is a much better result than the noCP MG3S value. Dunning's augmented basis sets were previously analyzed for the water dimer, and the recommendation still holds: noCP aTZ, noCP aQZ, and noCP a5Z are highly recommended, while the aDZ basis set should only be used with counterpoise corrections. If the aug-pc-X (X = 0, 1, 2, 3, 4) [acpX] basis sets[138–140] are desired, we recommend aug-pc-3 and aug-pc-4 without counterpoise corrections. aug-pc-0 should not be used and if aug-pc-1 and aug-pc-2 are desired, they should be used with counterpoise corrections. If the def2-X(Z)VP(P)D (X = S, T, Q) basis sets of Rappoport and Furche[78] are desired, we recommend using the def2-TZVPPD, def2-QZVPD, and def2-QZVPPD basis sets without counterpoise corrections. If calculations with the def2-TZVPD basis set are required, counterpoise corrections should be utilized. In addition, the def2-SVPD basis set should not be used with ωB97X-V. The last family of basis sets that was tested was Truhlar's minimally augmented basis set series,[141] maug-cc-pVXZ (X = D, T, Q) [maXZ]. Results with these basis sets indicated that only the maQZ basis set can be recommended with counterpoise corrections, while the maDZ and maTZ cannot be recommended for use with ωB97X-V.

Another looming question in the realm of DFT calculations is the proper choice for the integration grid. While ωB97X-V was trained with the (99,590) grid for the local exchange-correlation functional and the SG-1 grid for the nonlocal correlation functional, several tests were performed in order to quantify the extent to which the binding energies of weakly interacting systems depend on both the local and nonlocal integration grids. The tests were performed by combining 5 local grids {SG-1, (75,302), (99,590), (250,590), (500,974)} with 3 nonlocal grids {SG-1, (75,302), (99,590)}, for a total of fifteen distinct local and nonlocal grid combinations. Potential energy curves (PEC) for 2 families of dimers, as well as the water dimer, were computed with these fifteen grid combinations. The first family of dimers was

Table 10: Assessment of the basis set dependence of ωB97X-V for the binding energies of 3 dimers. Columns labeled BSSE contain the basis set superposition errors for the molecule/basis set combination indicated, columns labeled noCP contain non-counterpoise-corrected binding energies, while columns labeled CP contain counterpoise-corrected binding energies.

kcal/mol	$(H_2O)_2$			$(HF)_2$			$(NH_3)_2$		
Basis	BSSE	CP	noCP	BSSE	CP	noCP	BSSE	CP	noCP
MG3S	0.40	-5.03	-5.43	0.39	-4.56	-4.95	0.17	-3.18	-3.35
LP	0.29	-4.99	-5.28	0.38	-4.60	-4.98	0.10	-3.10	-3.21
aDZ	0.22	-4.96	-5.18	0.20	-4.54	-4.74	0.39	-3.06	-3.45
aTZ	0.05	-4.98	-5.03	0.07	-4.58	-4.65	0.03	-3.09	-3.12
aQZ	0.03	-5.01	-5.04	0.03	-4.64	-4.67	0.02	-3.10	-3.12
a5Z	0.01	-5.00	-5.01	0.01	-4.64	-4.64	0.00	-3.10	-3.10
apc0	1.48	-7.76	-9.24	0.85	-6.17	-7.02	1.29	-4.71	-5.99
apc1	0.65	-5.08	-5.73	0.63	-4.67	-5.30	0.53	-3.10	-3.63
apc2	0.06	-5.02	-5.08	0.10	-4.64	-4.74	0.05	-3.11	-3.15
apc3	0.00	-5.01	-5.01	0.00	-4.63	-4.64	0.00	-3.10	-3.10
apc4	0.00	-5.01	-5.01	0.00	-4.64	-4.64	0.00	-3.10	-3.10
svpd	0.41	-5.13	-5.54	0.41	-4.70	-5.10	0.74	-3.07	-3.81
tzvpd	0.07	-5.00	-5.06	0.05	-4.55	-4.60	0.13	-3.11	-3.23
tzvppd	0.03	-5.00	-5.03	0.03	-4.60	-4.63	0.09	-3.08	-3.17
qzvpd	0.01	-5.00	-5.01	0.01	-4.63	-4.64	0.02	-3.10	-3.11
qzvppd	0.01	-5.00	-5.01	0.01	-4.63	-4.64	0.02	-3.10	-3.11
maDZ	0.51	-5.28	-5.79	0.37	-4.54	-4.91	0.35	-3.36	-3.71
maTZ	0.16	-5.05	-5.21	0.09	-4.53	-4.62	0.13	-3.19	-3.32
maQZ	0.07	-5.03	-5.11	0.03	-4.62	-4.66	0.06	-3.13	-3.19

the rare-gas dimers from neon to krypton. The second family of dimers was CH_4—X, where X = F_2, Cl_2, and Br_2 (X40 dataset geometries). The def2-TZVPPD basis set was used for all of the calculations in this test. The PECs each had a total of 51 points, starting from a distance of 1 Å shorter than the equilibrium bond length, and continuing to 4 Å longer than the equilibrium bond length in increments of 0.1 Å. Thus, a total of 105 PECs were computed, requiring 5520 single-point calculations. For the first family of PECs, the ωB97X-V equilibrium binding energies in kcal/mol are $\{-0.13, -0.32, -0.42\}$, compared to the Tang-Toennies estimates of $\{-0.08, -0.28, -0.40\}$. For the second family of PECs, the ωB97X-V equilibrium binding energies in kcal/mol are $\{-0.48, -1.07, -1.31\}$, compared to the X40 estimates of $\{-0.49, -1.08, -1.30\}$. All of these interactions were assessed by calculating the percent error for each point on the fifteen PECs with respect to the (500,974)/(99,590) value, and computing the RMSDs of the 51 percent errors. Percent error RMSDs of approximately 1% or less were deemed acceptable.

Based on the data from Table 11, a minimum grid combination of (250,590)/(75,302) must be used for the neon and argon dimers. The krypton dimer calculations appear to be less sensitive to the nonlocal grid, and the (250,590)/SG-1 grid combination gives acceptable results. For the CH_4—X interactions, it appears as if the (99,590)/SG-1 grid combination gives unanimously acceptable results. Finally, for the water dimer (which binds at about -5.00 kcal/mol at equilibrium), using the SG-1 grid for both the local and nonlocal contributions is sufficient. Based on the results from Table 11, the following grids are recommended: (250,590)/(75,302) for interactions weaker than -0.5 kcal/mol at equilibrium, (99,590)/SG-1 for interactions between -0.5 kcal/mol and -2.5 kcal/mol at equilibrium, and (75,302)/SG-1 for interactions stronger than -2.5 kcal/mol at equilibrium.

Table 11: Assessment of the grid dependence of ωB97X-V for the potential energy curves of 7 dimers. The numbers shown are RMSDs of 51 percent errors. The percent errors are calculated by assuming that the (500,974)/(99,590) values are exact.

Ne_2	SG-1	(75,302)	(99,590)	(250,590)	(500,974)
SG-1	1539.82	54.43	34.67	18.67	18.46
(75,302)	1555.95	51.85	21.53	0.82	0.73
(99,590)	1556.16	52.14	21.12	0.50	0.00
Ar_2	SG-1	(75,302)	(99,590)	(250,590)	(500,974)
SG-1	575.68	18.18	8.16	6.53	6.62
(75,302)	581.11	18.22	4.13	0.20	0.23
(99,590)	581.22	57.31	4.01	0.16	0.00
Kr_2	SG-1	(75,302)	(99,590)	(250,590)	(500,974)
SG-1	58.36	10.15	2.90	0.89	0.83
(75,302)	58.75	9.67	2.64	0.33	0.11
(99,590)	58.73	9.70	2.65	0.31	0.00
CH_4F_2	SG-1	(75,302)	(99,590)	(250,590)	(500,974)
SG-1	2.67	0.27	0.14	0.10	0.10
(75,302)	2.67	0.28	0.09	0.05	0.05
(99,590)	2.69	0.28	0.09	0.01	0.00
CH_4Cl_2	SG-1	(75,302)	(99,590)	(250,590)	(500,974)
SG-1	11.52	0.36	0.17	0.15	0.15
(75,302)	11.59	0.37	0.10	0.05	0.05
(99,590)	11.60	0.34	0.09	0.01	0.00
CH_4Br_2	SG-1	(75,302)	(99,590)	(250,590)	(500,974)
SG-1	10.47	1.04	0.18	0.19	0.14
(75,302)	10.54	1.02	0.12	0.13	0.05
(99,590)	10.54	1.01	0.13	0.12	0.00
$(H_2O)_2$	SG-1	(75,302)	(99,590)	(250,590)	(500,974)
SG-1	0.15	0.01	0.01	0.01	0.01
(75,302)	0.15	0.01	0.01	0.01	0.00
(99,590)	0.14	0.01	0.01	0.01	0.00

As a reference value for those interested

in implementing this new density functional, the absolute energy (in hartrees) of hydrogen fluoride (HF) with a bond length of 0.9158 Å in the aug-cc-pVTZ basis set with the (75,302)/SG-1 local/nonlocal grid combination is -100.4512112969.

9 Conclusions

The primary goal of the development of the ωB97X-V density functional was to create a minimally-parameterized and highly-transferable density functional that could predict accurate energetics for both bonded and non-bonded interactions. With respect to thermochemistry, the performance of ωB97X-V is equivalent to that of ωB97X-D, despite the fact that ωB97X-V has 5 less empirical parameters. Furthermore, the performance of ωB97X-V on noncovalent interactions is considerably better than that of all the functionals tested in this paper. Table 12 ranks the 16 benchmarked density functionals with respect to their overall RMSDs for all of the bonded (1002) and non-bonded (1484) interactions considered in this paper.

To summarize the main results of this paper:

(1). We have optimized a new 10-parameter, semi-empirical density functional, ωB97X-V, that is a range-separated hybrid functional based on the B97 GGA model for local exchange and correlation, augmented with nonlocal correlation using the VV10 NLC functional.

(2). A novel feature of the training procedure is that over 16000 candidate functionals were trained and considered. By assessing their performance on both training and test set data, it was determined that 7 linear parameters yielded the most transferable functional. Increasing the number of parameters past 7 degraded test set performance and minimally improved training set performance.

(3). Detailed assessment against 15 existing density functionals on main group thermochemistry and noncovalent interactions suggests that ωB97X-V is the best functional tested for non-bonded interactions by a significant margin. Its performance for thermochemistry is also very good, virtually as good as the best hybrid meta-GGA tested (M06-2X).

Table 12: Density functionals ranked based on their overall unweighted RMSDs in kcal/mol for all thermochemistry (Columns 1-2) and noncovalent interactions (Columns 3-4) datapoints considered in this paper.

Functional	All TC	Functional	All NC
M06-2X	3.21	ωB97X-V	0.32
ωB97X-V	3.61	M06-L	0.47
ωB97X-D	3.61	B97-D2	0.48
B97-D2	3.97	ωB97X-D	0.54
M11	3.98	M11	0.56
M06	4.18	M06	0.60
B3LYP-D2	4.59	LC-VV10	0.73
B97	4.74	M06-2X	0.78
B3LYP	5.11	B97-D	0.82
B97-D	5.56	B3LYP-D2	1.01
M06-L	5.63	M11-L	1.07
M11-L	6.68	VV10	1.38
LC-VV10	6.80	PBE-D2	1.49
VV10	9.81	PBE	2.00
PBE	9.90	B97	2.71
PBE-D2	10.35	B3LYP	2.96

(4). ωB97X-V can be recommended for application to a wide range of molecular bonded and non-bonded interactions involving the lighter main group elements. It will be interesting to await further assessment on larger classes of problems in order to characterize its limitations. Such limitations are likely to arise for problems where strong correlation effects are in play.

(5). It is desirable to apply the same training approach used here to develop other semi-empirical density functionals with slightly different physical content (e.g. meta-GGAs), so that the resulting functionals are likewise optimally transferable. We intend to report such developments in due course.

10 Acknowledgements

This work was supported by the Director, Office of Energy Research, Office of Basic Energy Sciences, Chemical Sciences Division of the

U.S. Department of Energy under Contract DE-AC0376SF00098, and by a grant from the SciDac Program.

References

(1) Slater, J. C. A Simplification of the Hartree-Fock Method. *Phys. Rev.* **1951**, *81*, 385–390.

(2) Hohenberg, P.; Kohn, W. Inhomogeneous Electron Gas. *Phys. Rev.* **1964**, *136*, B864–B871.

(3) Kohn, W.; Sham, L. J. Self-Consistent Equations Including Exchange and Correlation Effects. *Phys. Rev.* **1965**, *140*, A1133–A1138.

(4) Becke, A. D. Density-functional thermochemistry. V. Systematic optimization of exchange-correlation functionals. *The Journal of Chemical Physics* **1997**, *107*, 8554–8560.

(5) Hamprecht, F. A.; Cohen, A. J.; Tozer, D. J.; Handy, N. C. Development and assessment of new exchange-correlation functionals. *The Journal of Chemical Physics* **1998**, *109*, 6264–6271.

(6) Zhao, Q.; Morrison, R. C.; Parr, R. G. From electron densities to Kohn-Sham kinetic energies, orbital energies, exchange-correlation potentials, and exchange-correlation energies. *Phys. Rev. A* **1994**, *50*, 2138–2142.

(7) Boese, A. D.; Doltsinis, N. L.; Handy, N. C.; Sprik, M. New generalized gradient approximation functionals. *The Journal of Chemical Physics* **2000**, *112*, 1670–1678.

(8) Boese, A. D.; Handy, N. C. A new parametrization of exchange–correlation generalized gradient approximation functionals. *The Journal of Chemical Physics* **2001**, *114*, 5497–5503.

(9) Wilson, P. J.; Bradley, T. J.; Tozer, D. J. Hybrid exchange-correlation functional determined from thermochemical data and ab initio potentials. *The Journal of Chemical Physics* **2001**, *115*, 9233–9242.

(10) Keal, T. W.; Tozer, D. J. Semiempirical hybrid functional with improved performance in an extensive chemical assessment. *The Journal of Chemical Physics* **2005**, *123*, 121103.

(11) Voorhis, T. V.; Scuseria, G. E. A novel form for the exchange-correlation energy functional. *The Journal of Chemical Physics* **1998**, *109*, 400–410.

(12) Becke, A. D. A new inhomogeneity parameter in density-functional theory. *The Journal of Chemical Physics* **1998**, *109*, 2092–2098.

(13) Becke, A. D.; Roussel, M. R. Exchange holes in inhomogeneous systems: A coordinate-space model. *Phys. Rev. A* **1989**, *39*, 3761–3767.

(14) Becke, A. D. Correlation energy of an inhomogeneous electron gas: A coordinate-space model. *The Journal of Chemical Physics* **1988**, *88*, 1053–1062.

(15) Boese, A. D.; Handy, N. C. New exchange-correlation density functionals: The role of the kinetic-energy density. *The Journal of Chemical Physics* **2002**, *116*, 9559–9569.

(16) Becke, A. D. Simulation of delocalized exchange by local density functionals. *The Journal of Chemical Physics* **2000**, *112*, 4020–4026.

(17) Tao, J.; Perdew, J. P.; Staroverov, V. N.; Scuseria, G. E. Climbing the Density Functional Ladder: Nonempirical Meta˘Generalized Gradient Approximation Designed for Molecules and Solids. *Phys. Rev. Lett.* **2003**, *91*, 146401.

(18) Boese, A. D.; Martin, J. M. L. Development of density functionals for thermochemical kinetics. *The Journal of Chemical Physics* **2004**, *121*, 3405–3416.

(19) Zhao, Y.; Truhlar, D. G. A new local density functional for main-group thermochemistry, transition metal bonding, thermochemical kinetics, and noncovalent interactions. *The Journal of Chemical Physics* **2006**, *125*, 194101.

(20) Peverati, R.; Truhlar, D. G. M11-L: A Local Density Functional That Provides Improved Accuracy for Electronic Structure Calculations in Chemistry and Physics. *The Journal of Physical Chemistry Letters* **2012**, *3*, 117–124.

(21) Zhao, Y.; Schultz, N. E.; Truhlar, D. G. Exchange-correlation functional with broad accuracy for metallic and nonmetallic compounds, kinetics, and noncovalent interactions. *The Journal of Chemical Physics* **2005**, *123*, 161103.

(22) Zhao, Y.; Schultz, N. E.; Truhlar, D. G. Design of Density Functionals by Combining the Method of Constraint Satisfaction with Parametrization for Thermochemistry, Thermochemical Kinetics, and Noncovalent Interactions. *Journal of Chemical Theory and Computation* **2006**, *2*, 364–382.

(23) Zhao, Y.; Truhlar, D. The M06 suite of density functionals for main group thermochemistry, thermochemical kinetics, noncovalent interactions, excited states, and transition elements: two new functionals and systematic testing of four M06-class functionals and 12 other functionals. *Theoretical Chemistry Accounts: Theory, Computation, and Modeling (Theoretica Chimica Acta)* **2008**, *120*, 215–241.

(24) Zhao, Y.; Truhlar, D. G. Density Functional for Spectroscopy: No Long-Range Self-Interaction Error, Good Performance for Rydberg and Charge-Transfer States, and Better Performance on Average than B3LYP for Ground States. *The Journal of Physical Chemistry A* **2006**, *110*, 13126–13130.

(25) Zhao, Y.; Truhlar, D. G. Exploring the Limit of Accuracy of the Global Hybrid Meta Density Functional for Main-Group Thermochemistry, Kinetics, and Noncovalent Interactions. *Journal of Chemical Theory and Computation* **2008**, *4*, 1849–1868.

(26) Peverati, R.; Truhlar, D. G. Improving the Accuracy of Hybrid Meta-GGA Density Functionals by Range Separation. *The Journal of Physical Chemistry Letters* **2011**, *2*, 2810–2817.

(27) Hammer, B.; Hansen, L. B.; Nørskov, J. K. Improved adsorption energetics within density-functional theory using revised Perdew-Burke-Ernzerhof functionals. *Phys. Rev. B* **1999**, *59*, 7413–7421.

(28) Perdew, J. P.; Zunger, A. Self-interaction correction to density-functional approximations for many-electron systems. *Phys. Rev. B* **1981**, *23*, 5048–5079.

(29) Leininger, T.; Stoll, H.; Werner, H.-J.; Savin, A. Combining long-range configuration interaction with short-range density functionals. *Chemical Physics Letters* **1997**, *275*, 151 – 160.

(30) Iikura, H.; Tsuneda, T.; Yanai, T.; Hirao, K. A long-range correction scheme for generalized-gradient-approximation exchange functionals. *The Journal of Chemical Physics* **2001**, *115*, 3540–3544.

(31) Becke, A. D. Density-functional exchange-energy approximation with correct asymptotic behavior. *Phys. Rev. A* **1988**, *38*, 3098–3100.

(32) Tsuneda, T.; Hirao, K. A new spin-polarized Colle-Salvetti-type correlation

energy functional. *Chemical Physics Letters* **1997**, *268*, 510 – 520.

(33) Tsuneda, T.; Suzumura, T.; Hirao, K. A new one-parameter progressive Colle–Salvetti-type correlation functional. *The Journal of Chemical Physics* **1999**, *110*, 10664–10678.

(34) Tawada, Y.; Tsuneda, T.; Yanagisawa, S.; Yanai, T.; Hirao, K. A long-range-corrected time-dependent density functional theory. *The Journal of Chemical Physics* **2004**, *120*, 8425–8433.

(35) Gill, P. M. W.; Adamson, R. D.; Pople, J. A. Coulomb-attenuated exchange energy density functionals. *Molecular Physics* **1996**, *88*, 1005–1009.

(36) Vydrov, O. A.; Scuseria, G. E. Assessment of a long-range corrected hybrid functional. *The Journal of Chemical Physics* **2006**, *125*, 234109.

(37) Vydrov, O. A.; Heyd, J.; Krukau, A. V.; Scuseria, G. E. Importance of short-range versus long-range Hartree-Fock exchange for the performance of hybrid density functionals. *The Journal of Chemical Physics* **2006**, *125*, 074106.

(38) Henderson, T. M.; Janesko, B. G.; Scuseria, G. E. Generalized gradient approximation model exchange holes for range-separated hybrids. *The Journal of Chemical Physics* **2008**, *128*, 194105.

(39) Weintraub, E.; Henderson, T. M.; Scuseria, G. E. Long-Range-Corrected Hybrids Based on a New Model Exchange Hole. *Journal of Chemical Theory and Computation* **2009**, *5*, 754–762.

(40) Rohrdanz, M. A.; Herbert, J. M. Simultaneous benchmarking of ground- and excited-state properties with long-range-corrected density functional theory. *The Journal of Chemical Physics* **2008**, *129*, 034107.

(41) Rohrdanz, M. A.; Martins, K. M.; Herbert, J. M. A long-range-corrected density functional that performs well for both ground-state properties and time-dependent density functional theory excitation energies, including charge-transfer excited states. *The Journal of Chemical Physics* **2009**, *130*, 054112.

(42) Chai, J.-D.; Head-Gordon, M. Systematic optimization of long-range corrected hybrid density functionals. *The Journal of Chemical Physics* **2008**, *128*, 084106.

(43) Chai, J.-D.; Head-Gordon, M. Long-range corrected hybrid density functionals with damped atom-atom dispersion corrections. *Phys. Chem. Chem. Phys.* **2008**, *10*, 6615–6620.

(44) Kristyan, S.; Pulay, P. Can (semi)local density functional theory account for the London dispersion forces? *Chemical Physics Letters* **1994**, *229*, 175 – 180.

(45) Hobza, P.; Šponer, J.; Reschel, T. Density functional theory and molecular clusters. *J. Comput. Chem.* **1995**, *16*, 1315–1325.

(46) Klimeš, J.; Michaelides, A. Perspective: Advances and challenges in treating van der Waals dispersion forces in density functional theory. *The Journal of Chemical Physics* **2012**, *137*, 120901.

(47) Grimme, S. Accurate description of van der Waals complexes by density functional theory including empirical corrections. *J. Comput. Chem.* **2004**, *25*, 1463–1473.

(48) Grimme, S. Semiempirical GGA-type density functional constructed with a long-range dispersion correction. *Journal of Computational Chemistry* **2006**, *27*, 1787–1799.

(49) Grimme, S.; Antony, J.; Ehrlich, S.; Krieg, H. A consistent and accurate ab initio parametrization of density functional dispersion correction (DFT-D) for

the 94 elements H-Pu. *The Journal of Chemical Physics* **2010**, *132*, 154104.

(50) Jurečka, P.; Černý, J.; Hobza, P.; Salahub, D. R. Density functional theory augmented with an empirical dispersion term. Interaction energies and geometries of 80 noncovalent complexes compared with ab initio quantum mechanics calculations. *J. Comput. Chem.* **2007**, *28*, 555–569.

(51) Becke, A. D.; Johnson, E. R. A density-functional model of the dispersion interaction. *The Journal of Chemical Physics* **2005**, *123*, 154101.

(52) Becke, A. D.; Johnson, E. R. Exchange-hole dipole moment and the dispersion interaction. *The Journal of Chemical Physics* **2005**, *122*, 154104.

(53) Johnson, E. R.; Becke, A. D. A post-Hartree–Fock model of intermolecular interactions. *The Journal of Chemical Physics* **2005**, *123*, 024101.

(54) Becke, A. D.; Johnson, E. R. Exchange-hole dipole moment and the dispersion interaction: High-order dispersion coefficients. *The Journal of Chemical Physics* **2006**, *124*, 014104.

(55) Johnson, E. R.; Becke, A. D. A post-Hartree-Fock model of intermolecular interactions: Inclusion of higher-order corrections. *The Journal of Chemical Physics* **2006**, *124*, 174104.

(56) Johnson, E. R.; Becke, A. D. Van der Waals interactions from the exchange hole dipole moment: Application to bio-organic benchmark systems. *Chemical Physics Letters* **2006**, *432*, 600 – 603.

(57) Becke, A. D.; Johnson, E. R. Exchange-hole dipole moment and the dispersion interaction revisited. *The Journal of Chemical Physics* **2007**, *127*, 154108.

(58) Kong, J.; Gan, Z.; Proynov, E.; Freindorf, M.; Furlani, T. R. Efficient computation of the dispersion interaction with density-functional theory. *Phys. Rev. A* **2009**, *79*, 042510.

(59) Dion, M.; Rydberg, H.; Schröder, E.; Langreth, D. C.; Lundqvist, B. I. Van der Waals Density Functional for General Geometries. *Phys. Rev. Lett.* **2004**, *92*, 246401.

(60) Lee, K.; Murray, E. D.; Kong, L.; Lundqvist, B. I.; Langreth, D. C. Higher-accuracy van der Waals density functional. *Phys. Rev. B* **2010**, *82*, 081101.

(61) Vydrov, O. A.; Van Voorhis, T. Nonlocal van der Waals Density Functional Made Simple. *Phys. Rev. Lett.* **2009**, *103*, 063004.

(62) Vydrov, O. A.; Voorhis, T. V. Nonlocal van der Waals density functional: The simpler the better. *The Journal of Chemical Physics* **2010**, *133*, 244103.

(63) Vydrov, O. A.; Wu, Q.; Voorhis, T. V. Self-consistent implementation of a nonlocal van der Waals density functional with a Gaussian basis set. *The Journal of Chemical Physics* **2008**, *129*, 014106.

(64) Vydrov, O. A.; Voorhis, T. V. Improving the accuracy of the nonlocal van der Waals density functional with minimal empiricism. *The Journal of Chemical Physics* **2009**, *130*, 104105.

(65) Vydrov, O. A.; Voorhis, T. V. Implementation and assessment of a simple nonlocal van der Waals density functional. *The Journal of Chemical Physics* **2010**, *132*, 164113.

(66) Vydrov, O. A.; Van Voorhis, T. Dispersion interactions from a local polarizability model. *Phys. Rev. A* **2010**, *81*, 062708.

(67) Perdew, J. P.; Ruzsinszky, A.; Tao, J.; Staroverov, V. N.; Scuseria, G. E.;

Csonka, G. I. Prescription for the design and selection of density functional approximations: More constraint satisfaction with fewer fits. *The Journal of Chemical Physics* **2005**, *123*, 062201.

(68) Johnson, E. R.; Wolkow, R. A.; DiLabio, G. A. Application of 25 density functionals to dispersion-bound homomolecular dimers. *Chemical Physics Letters* **2004**, *394*, 334 – 338.

(69) Grafenstein, J.; Izotov, D.; Cremer, D. Avoiding singularity problems associated with meta-GGA (generalized gradient approximation) exchange and correlation functionals containing the kinetic energy density. *The Journal of Chemical Physics* **2007**, *127*, 214103.

(70) Johnson, E. R.; Becke, A. D.; Sherrill, C. D.; DiLabio, G. A. Oscillations in meta-generalized-gradient approximation potential energy surfaces for dispersion-bound complexes. *The Journal of Chemical Physics* **2009**, *131*, 034111.

(71) Wheeler, S. E.; Houk, K. N. Integration Grid Errors for Meta-GGA-Predicted Reaction Energies: Origin of Grid Errors for the M06 Suite of Functionals. *Journal of Chemical Theory and Computation* **2010**, *6*, 395–404.

(72) Mardirossian, N.; Lambrecht, D. S.; McCaslin, L.; Xantheas, S. S.; Head-Gordon, M. The Performance of Density Functionals for SulfateWater Clusters. *Journal of Chemical Theory and Computation* **2013**, *9*, 1368–1380.

(73) Gill, P. M.; Johnson, B. G.; Pople, J. A. A standard grid for density functional calculations. *Chemical Physics Letters* **1993**, *209*, 506 – 512.

(74) Thom H. Dunning, J. Gaussian basis sets for use in correlated molecular calculations. I. The atoms boron through neon and hydrogen. *The Journal of Chemical Physics* **1989**, *90*, 1007–1023.

(75) Woon, D. E.; Thom H. Dunning, J. Gaussian basis sets for use in correlated molecular calculations. III. The atoms aluminum through argon. *The Journal of Chemical Physics* **1993**, *98*, 1358–1371.

(76) Řezáč, J.; Riley, K. E.; Hobza, P. Benchmark Calculations of Noncovalent Interactions of Halogenated Molecules. *Journal of Chemical Theory and Computation* **2012**, *8*, 4285–4292.

(77) Peterson, K. A.; Figgen, D.; Goll, E.; Stoll, H.; Dolg, M. Systematically convergent basis sets with relativistic pseudopotentials. II. Small-core pseudopotentials and correlation consistent basis sets for the post-d group 16–18 elements. *The Journal of Chemical Physics* **2003**, *119*, 11113–11123.

(78) Rappoport, D.; Furche, F. Property-optimized Gaussian basis sets for molecular response calculations. *The Journal of Chemical Physics* **2010**, *133*, 134105.

(79) Burns, L. A.; Álvaro Vázquez-Mayagoitia,; Sumpter, B. G.; Sherrill, C. D. Density-functional approaches to noncovalent interactions: A comparison of dispersion corrections (DFT-D), exchange-hole dipole moment (XDM) theory, and specialized functionals. *The Journal of Chemical Physics* **2011**, *134*, 084107.

(80) Shao, Y.; Molnar, L. F.; Jung, Y.; Kussmann, J.; Ochsenfeld, C.; Brown, S. T.; Gilbert, A. T.; Slipchenko, L. V.; Levchenko, S. V.; O'Neill, D. P. et al. Advances in methods and algorithms in a modern quantum chemistry program package. *Phys. Chem. Chem. Phys.* **2006**, *8*, 3172–3191.

(81) Becke, A. D. Density functional calculations of molecular bond energies. *The Journal of Chemical Physics* **1986**, *84*, 4524–4529.

(82) Ceperley, D. M.; Alder, B. J. Ground State of the Electron Gas by a Stochastic Method. *Phys. Rev. Lett.* **1980**, *45*, 566–569.

(83) Perdew, J. P.; Wang, Y. Accurate and simple analytic representation of the electron-gas correlation energy. *Phys. Rev. B* **1992**, *45*, 13244–13249.

(84) Vosko, S. H.; Wilk, L.; Nusair, M. Accurate spin-dependent electron liquid correlation energies for local spin density calculations: a critical analysis. *Can. J. Phys.* **1980**, *58*, 1200–1211.

(85) Stoll, H.; Golka, E.; Preuß, H. Correlation energies in the spin-density functional formalism. *Theoretical Chemistry Accounts: Theory, Computation, and Modeling (Theoretica Chimica Acta)* **1980**, *55*, 29–41.

(86) Karton, A.; Tarnopolsky, A.; Lamère, J.-F.; Schatz, G. C.; Martin, J. M. L. Highly Accurate First-Principles Benchmark Data Sets for the Parametrization and Validation of Density Functional and Other Approximate Methods. Derivation of a Robust, Generally Applicable, Double-Hybrid Functional for Thermochemistry and Thermochemical Kinetics. *The Journal of Physical Chemistry A* **2008**, *112*, 12868–12886.

(87) Chakravorty, S. J.; Gwaltney, S. R.; Davidson, E. R.; Parpia, F. A.; p Fischer, C. F. Ground-state correlation energies for atomic ions with 3 to 18 electrons. *Phys. Rev. A* **1993**, *47*, 3649–3670.

(88) Karton, A.; Gruzman, D.; Martin, J. M. L. Benchmark Thermochemistry of the CnH2n+2 Alkane Isomers (n = 28) and Performance of DFT and Composite Ab Initio Methods for Dispersion-Driven Isomeric Equilibria. *The Journal of Physical Chemistry A* **2009**, *113*, 8434–8447.

(89) Copeland, K. L.; Tschumper, G. S. Hydrocarbon/Water Interactions: Encouraging Energetics and Structures from DFT but Disconcerting Discrepancies for Hessian Indices. *Journal of Chemical Theory and Computation* **2012**, *8*, 1646–1656.

(90) Zhao, Y.; Truhlar, D. G. Benchmark Databases for Nonbonded Interactions and Their Use To Test Density Functional Theory. *Journal of Chemical Theory and Computation* **2005**, *1*, 415–432.

(91) Lao, K. U.; Herbert, J. M. An improved treatment of empirical dispersion and a many-body energy decomposition scheme for the explicit polarization plus symmetry-adapted perturbation theory (XSAPT) method. *The Journal of Chemical Physics* **2013**, *139*, 034107.

(92) Zheng, J.; Zhao, Y.; Truhlar, D. G. Representative Benchmark Suites for Barrier Heights of Diverse Reaction Types and Assessment of Electronic Structure Methods for Thermochemical Kinetics. *Journal of Chemical Theory and Computation* **2007**, *3*, 569–582.

(93) Brittain, D. R. B.; Lin, C. Y.; Gilbert, A. T. B.; Izgorodina, E. I.; Gill, P. M. W.; Coote, M. L. The role of exchange in systematic DFT errors for some organic reactions. *Phys. Chem. Chem. Phys.* **2009**, *11*, 1138–1142.

(94) Zhao, Y.; Lynch, B. J.; Truhlar, D. G. Multi-coefficient extrapolated density functional theory for thermochemistry and thermochemical kinetics. *Phys. Chem. Chem. Phys.* **2005**, *7*, 43–52.

(95) Zhao, Y.; González-García, N.; Truhlar, D. G. Benchmark Database of Barrier Heights for Heavy Atom Transfer, Nucleophilic Substitution, Association, and Unimolecular Reactions and Its Use

to Test Theoretical Methods. *The Journal of Physical Chemistry A* **2005**, *109*, 2012–2018.

(96) Gráfová, L.; Pitoňák, M.; Řezáč, J.; Hobza, P. Comparative Study of Selected Wave Function and Density Functional Methods for Noncovalent Interaction Energy Calculations Using the Extended S22 Data Set. *Journal of Chemical Theory and Computation* **2010**, *6*, 2365–2376.

(97) Parthiban, S.; Martin, J. M. L. Assessment of W1 and W2 theories for the computation of electron affinities, ionization potentials, heats of formation, and proton affinities. *The Journal of Chemical Physics* **2001**, *114*, 6014–6029.

(98) Zhao, Y.; Truhlar, D. G. Assessment of Density Functionals for Systems: Energy Differences between Cumulenes and Poly-ynes; Proton Affinities, Bond Length Alternation, and Torsional Potentials of Conjugated Polyenes; and Proton Affinities of Conjugated Shiff Bases. *The Journal of Physical Chemistry A* **2006**, *110*, 10478–10486.

(99) Wilke, J. J.; Lind, M. C.; Schaefer, H. F.; Csaszar, A. G.; Allen, W. D. Conformers of Gaseous Cysteine. *Journal of Chemical Theory and Computation* **2009**, *5*, 1511–1523.

(100) Thanthiriwatte, K. S.; Hohenstein, E. G.; Burns, L. A.; Sherrill, C. D. Assessment of the Performance of DFT and DFT-D Methods for Describing Distance Dependence of Hydrogen-Bonded Interactions. *Journal of Chemical Theory and Computation* **2011**, *7*, 88–96.

(101) Hohenstein, E. G.; Sherrill, C. D. Effects of Heteroatoms on Aromatic Interactions: BenzenePyridine and Pyridine Dimer. *The Journal of Physical Chemistry A* **2009**, *113*, 878–886.

(102) Sherrill, C. D.; Takatani, T.; Hohenstein, E. G. An Assessment of Theoretical Methods for Nonbonded Interactions: Comparison to Complete Basis Set Limit Coupled-Cluster Potential Energy Curves for the Benzene Dimer, the Methane Dimer, BenzeneMethane, and BenzeneH2S. *The Journal of Physical Chemistry A* **2009**, *113*, 10146–10159.

(103) Lynch, B. J.; Truhlar, D. G. Robust and Affordable Multicoefficient Methods for Thermochemistry and Thermochemical Kinetics: The MCCM/3 Suite and SAC/3. *The Journal of Physical Chemistry A* **2003**, *107*, 3898–3906.

(104) Karton, A.; Daon, S.; Martin, J. M. W4-11: A high-confidence benchmark dataset for computational thermochemistry derived from first-principles {W4} data. *Chemical Physics Letters* **2011**, *510*, 165 – 178.

(105) Curtiss, L. A.; Raghavachari, K.; Trucks, G. W.; Pople, J. A. Gaussian-2 theory for molecular energies of first- and second-row compounds. *The Journal of Chemical Physics* **1991**, *94*, 7221–7230.

(106) Dahlke, E. E.; Olson, R. M.; Leverentz, H. R.; Truhlar, D. G. Assessment of the Accuracy of Density Functionals for Prediction of Relative Energies and Geometries of Low-Lying Isomers of Water Hexamers. *The Journal of Physical Chemistry A* **2008**, *112*, 3976–3984.

(107) Bates, D. M.; Tschumper, G. S. CCSD(T) Complete Basis Set Limit Relative Energies for Low-Lying Water Hexamer Structures. *The Journal of Physical Chemistry A* **2009**, *113*, 3555–3559.

(108) Řezáč, J.; Hobza, P. Describing Noncovalent Interactions beyond the Common Approximations: How Accurate Is the Gold Standard CCSD(T) at the Complete Basis Set Limit? *Journal of Chemical Theory and Computation* **2013**, *9*, 2151–2155.

(109) Mintz, B. J.; Parks, J. M. Benchmark Interaction Energies for Biologically Relevant Noncovalent Complexes Containing Divalent Sulfur. *The Journal of Physical Chemistry A* **2012**, *116*, 1086–1092.

(110) Bryantsev, V. S.; Diallo, M. S.; van Duin, A. C. T.; Goddard, W. A. Evaluation of B3LYP, X3LYP, and M06-Class Density Functionals for Predicting the Binding Energies of Neutral, Protonated, and Deprotonated Water Clusters. *Journal of Chemical Theory and Computation* **2009**, *5*, 1016–1026.

(111) Goerigk, L.; Grimme, S. A thorough benchmark of density functional methods for general main group thermochemistry, kinetics, and noncovalent interactions. *Phys. Chem. Chem. Phys.* **2011**, *13*, 6670–6688.

(112) Jurečka, P.; Šponer, J.; Černý, J.; Hobza, P. Benchmark database of accurate (MP2 and CCSD(T) complete basis set limit) interaction energies of small model complexes, DNA base pairs, and amino acid pairs. *Phys. Chem. Chem. Phys.* **2006**, *8*, 1985–1993.

(113) Řezáč, J.; Riley, K. E.; Hobza, P. S66: A Well-balanced Database of Benchmark Interaction Energies Relevant to Biomolecular Structures. *Journal of Chemical Theory and Computation* **2011**, *7*, 2427–2438.

(114) Řezáč, J.; Riley, K. E.; Hobza, P. Extensions of the S66 Data Set: More Accurate Interaction Energies and Angular-Displaced Nonequilibrium Geometries. *Journal of Chemical Theory and Computation* **2011**, *7*, 3466–3470.

(115) Marshall, M. S.; Burns, L. A.; Sherrill, C. D. Basis set convergence of the coupled-cluster correction, delta[sub MP2][sup CCSD(T)]: Best practices for benchmarking non-covalent interactions and the attendant revision of the S22, NBC10, HBC6, and HSG databases. *The Journal of Chemical Physics* **2011**, *135*, 194102.

(116) Tang, K. T.; Toennies, J. P. The van der Waals potentials between all the rare gas atoms from He to Rn. *The Journal of Chemical Physics* **2003**, *118*, 4976–4983.

(117) Crittenden, D. L. A Systematic CCSD(T) Study of Long-Range and Noncovalent Interactions between Benzene and a Series of First- and Second-Row Hydrides and Rare Gas Atoms. *The Journal of Physical Chemistry A* **2009**, *113*, 1663–1669.

(118) Kendall, R. A.; Thom H. Dunning, J.; Harrison, R. J. Electron affinities of the first-row atoms revisited. Systematic basis sets and wave functions. *The Journal of Chemical Physics* **1992**, *96*, 6796–6806.

(119) Pekeris, C. L. 1^1S and 2^3S States of Helium. *Phys. Rev.* **1959**, *115*, 1216–1221.

(120) Lieb, E. H.; Oxford, S. Improved lower bound on the indirect Coulomb energy. *Int. J. Quantum Chem.* **1981**, *19*, 427–439.

(121) Zupan, A.; Perdew, J. P.; Burke, K.; Causa, M. Density-gradient analysis for density functional theory: Application to atoms. *Int. J. Quantum Chem.* **1997**, *61*, 835–845.

(122) Amovilli, C.; March, N.; Bogár, F.; Gál, T. Use of ab initio methods to classify four existing energy density functionals according to their possible variational validity. *Physics Letters A* **2009**, *373*, 3158 – 3160.

(123) Malli, G. L.; Da Silva, A. B. F.; Ishikawa, Y. Universal Gaussian basis set for accurate *ab initio* /P *relat ivistic* D *irac - Fock calculations. Phys. Rev. A* **1993**, *47*, 143–146.

(124) Perdew, J. P.; Burke, K.; Ernzerhof, M. Generalized Gradient Approximation Made Simple. *Phys. Rev. Lett.* **1996**, *77*, 3865–3868.

(125) Becke, A. D. Density-functional thermochemistry. III. The role of exact exchange. *The Journal of Chemical Physics* **1993**, *98*, 5648–5652.

(126) Janowski, T.; Ford, A. R.; Pulay, P. Accurate correlated calculation of the intermolecular potential surface in the coronene dimer. *Molecular Physics* **2010**, *108*, 249–257.

(127) Sedlak, R.; Janowski, T.; Pitoňák, M.; Řezáč, J.; Pulay, P.; Hobza, P. Accuracy of Quantum Chemical Methods for Large Noncovalent Complexes. *Journal of Chemical Theory and Computation* **2013**, *9*, 3364–3374.

(128) Goldey, M.; Dutoi, A.; Head-Gordon, M. Attenuated second-order Moller-Plesset perturbation theory: performance within the aug-cc-pVTZ basis. *Phys. Chem. Chem. Phys.* **2013**, *15*, 15869–15875.

(129) Pitoňák, M.; Neogrády, P.; Černý, J.; Grimme, S.; Hobza, P. Scaled MP3 Non-Covalent Interaction Energies Agree Closely with Accurate CCSD(T) Benchmark Data. *ChemPhysChem* **2009**, *10*, 282–289.

(130) Kabsch, W. A solution for the best rotation to relate two sets of vectors. *Acta Crystallographica Section A* **1976**, *32*, 922–923.

(131) Tentscher, P. R.; Arey, J. S. Geometries and Vibrational Frequencies of Small Radicals: Performance of Coupled Cluster and More Approximate Methods. *Journal of Chemical Theory and Computation* **2012**, *8*, 2165–2179.

(132) Bak, K. L.; Gauss, J.; Jørgensen, P.; Olsen, J.; Helgaker, T.; Stanton, J. F. The accurate determination of molecular equilibrium structures. *The Journal of Chemical Physics* **2001**, *114*, 6548–6556.

(133) Feller, D. The role of databases in support of computational chemistry calculations. *J. Comput. Chem.* **1996**, *17*, 1571–1586.

(134) Schuchardt, K. L.; Didier, B. T.; Elsethagen, T.; Sun, L.; Gurumoorthi, V.; Chase, J.; Li, J.; Windus, T. L. Basis Set Exchange: A Community Database for Computational Sciences. *Journal of Chemical Information and Modeling* **2007**, *47*, 1045–1052.

(135) Lynch, B. J.; Zhao, Y.; Truhlar, D. G. Effectiveness of Diffuse Basis Functions for Calculating Relative Energies by Density Functional Theory. *The Journal of Physical Chemistry A* **2003**, *107*, 1384–1388.

(136) Frisch, M. J.; Pople, J. A.; Binkley, J. S. Self-consistent molecular orbital methods 25. Supplementary functions for Gaussian basis sets. *The Journal of Chemical Physics* **1984**, *80*, 3265–3269.

(137) Krishnan, R.; Binkley, J. S.; Seeger, R.; Pople, J. A. Self-consistent molecular orbital methods. XX. A basis set for correlated wave functions. *The Journal of Chemical Physics* **1980**, *72*, 650–654.

(138) Jensen, F. Polarization consistent basis sets: Principles. *The Journal of Chemical Physics* **2001**, *115*, 9113–9125.

(139) Jensen, F. Polarization consistent basis sets. II. Estimating the Kohn–Sham basis set limit. *The Journal of Chemical Physics* **2002**, *116*, 7372–7379.

(140) Jensen, F. Polarization consistent basis sets. III. The importance of diffuse functions. *The Journal of Chemical Physics* **2002**, *117*, 9234–9240.

(141) Papajak, E.; Leverentz, H. R.; Zheng, J.; Truhlar, D. G. Efficient Diffuse Basis Sets: cc-pVxZ+ and maug-cc-pVxZ.

Journal of Chemical Theory and Computation **2009**, *5*, 3330–3330.